Development of a torque steer analysis tool for electric vehicles

van Es, Mitchell

Award date:
2022

Automotive Technology
Department of Mechanical Engineering
Dynamics and Control

Graduation Project

Development of a torque steer analysis tool for electric vehicles

D&C NR: 2022.102

Student:

Mitchell van Es (1243056)	m.v.es@student.tue.nl

Supervisors:

Ralf van Gestel	rvangestel@tesla.com
Chris Wouters	cwouters@tesla.com
Igo Besselink	I.J.M.Besselink@tue.nl

Eindhoven, January 20, 2023

Abstract

Torque steer on front-wheel drive vehicles is not uncommon. The tugging or jerking steering behaviour resulting from the torque produced by the motor is regarded as undesirable as it may disturb the driver and causes the vehicle to deviate from its intended path. With the rise of electric vehicles, the issue of torque steer becomes more prominent as the electric motor tend to produce a lot of torque instantaneously. Consequently, torque steer becomes more pronounced.

The goal of this project is to investigate- and ultimately prevent the torque steer experienced in electric vehicles. A generic multi-body model of a vehicle has been developed to analyse the behaviour. The model can be tailored to represent various vehicles through parameter changes. The model has been adjusted to the specification of the Tesla Model S, as this is the subject of this research.

Through the development and analysis of the model, root causes for torque steer have been found. The deflection of the motor mount during acceleration causes different inclination angles for the left and right half shafts. Furthermore, the differential was found to bias torque, like a limited-slip differential, to the slower wheel. Lastly, the air suspension was found to have asymmetrical air spring pressures. This results in an increased load on the front right and rear left tires provoking a wheel speed difference, which allows the differential to bias torque even when driving in a straight line.

The torque steer can be eliminated by redesigning the motor mounts and differential. The new design should include motor mounts with a horizontal torque roll axis and a differential which is closer to an open differential. This does, however, not alleviate torque steer for the vehicles currently in the fleet. Simulation and experiments have shown that lowering the pressure of the rear left air spring below that of the rear right air spring will result in the vehicle driving straight during hard acceleration. This will invert the torque steer produced by the differential which will then cancel out the torque steer produced by the asymmetric motor mount.

Nomenclature

Δ_ω	Wheel speed delta [rad/s]
δ_{sw}	Steering wheel angle. Right is positive [deg]
γ_{epas}	Gear ratio of the steering rack assist motor [-]
λ	Kingpin inclination angle [rad]
μ	Coefficient of friction [-]
ν	Caster angle [rad]
ω	Wheel speed [rad/s]
ω_{em}	Motor speed [rad/s]
ξ	Half shaft inclination angle [rad]
e_κ	TC/ABS control error [-]
A	Air spring effective surface area [m^2]
a_x	Longitudinal chassis acceleration [m/s^2]
a_y	Lateral chassis acceleration [m/s^2]
a_z	Vertical chassis acceleration [m/s^2]
F_s	Spring force [N]
F_x	Tractive tire force [N]
F_y	Lateral tire force [N]
F_z	The vertical tire force [N]
G_{bias}	Torque bias gain [-]
L_{epas}	Screw lead of the steering rack [m/rev]
M_{cv2nd}	The secondary moment generated by the CV joint [Nm]
M_t	Moment around the spindle generated by the tractive force [Nm]
M_x	The overturning moment of the tire [Nm]
M_y	The drive torque of the tire [Nm]
M_z	The self-aligning moment of the tire [Nm]
p	Air spring pressure [bar]
p_b	Atmospheric pressure [bar]
r_{pinion}	Radius of the pinion of the steering rack assist motor effective gear ratio [m]
r_w	Dynamic wheel radius [m]
r_{wco}	Wheel centre offset with respect to the centre of the kingpin [m]
T_{bias}	Differential torque bias [Nm]
T_{em}	Motor torque [Nm]

T_l	Left drive shaft torque [Nm]
T_r	Right drive shaft torque [Nm]
T_{sw}	Steering wheel angle torque. Right is positive [Nm]
u_{kp}	The unit vector of the kingpin axis [-]
V	Air volume [m^3]
$\|\|$	projection on the kingpin axis

Glossary

ABS Anti-lock Brake System.

CV joint Constant velocity joint.

EPAS Electric power-assisted steering.

ESP Electronic Stability Program.

NVH noise, vibration and harshness.

TC Traction Control.

Contents

Nomenclature **iii**

Glossary **iv**

1 Introduction **1**
1.1 Background . . . 1
1.2 Objectives . . . 1
1.3 Contributions . . . 1
1.4 Thesis Outline . . . 2

2 Literature Review **3**
2.1 Root Causes of Torque Steer . . . 3
2.2 Torque Steer Reduction . . . 6

3 Torque Steer Analysis Tool **8**
3.1 Model Development Approach . . . 8
3.2 Vehicle Data . . . 9
3.3 Suspension and Tires . . . 9
3.4 Springs and Dampers . . . 16
3.5 Steering System . . . 18
3.6 Motor Mounts . . . 22
3.7 Powertrain . . . 25
3.8 Full Vehicle Validation . . . 30

4 Torque Steer Testing Results **32**
4.1 Quantification . . . 32
4.2 Simulations . . . 32
4.2.1 Torque Steer Contributors . . . 32
4.2.2 Torque Steer Mitigation Strategies . . . 35
4.3 Experiments . . . 38

5 Conclusions & Recommendations **41**
5.1 Conclusions . . . 41
5.2 Recommendations . . . 41

References **43**

A Appendix **44**
A.1 Torque Steer Simulation Tool Instructions . . . 44
A.2 Full vehicle model hands off wide open throttle simulation results . . . 47
A.3 Model 3 motor mount hands off wide open throttle simulation results . . . 50
A.4 Adjusted air suspension hands off wide open throttle simulation results . . . 53

1 Introduction

1.1 Background

Torque steer is a characteristic that has been present in front-wheel drive vehicles for decades. It is defined as a tugging or jerking sensation on the steering wheel caused by the torque produced by the drive unit [1]. This behaviour can be disturbing to a driver as the steering wheel might pull aggressively to one side during harsh acceleration possibly resulting in the vehicle deviating from its intended path.

The torque steer effects became more noticeable with the rise of diesel engines producing increasing amounts of torque. Research into the root causes and suspension designs to reduce or eliminate torque steer has been conducted extensively. With the transition to electric vehicles, torque steer could again be on the rise as several models feature a drive unit driving the front wheels which may be capable of producing a lot of torque. This might result in torque steer being more noticeable in these types of vehicles.

The all-wheel drive Tesla Model S is one such vehicle which exhibits torque steer. In particular, the higher-performant configurations experience it to a greater extent. As a result, the manufacturer decided to move the drive torque split more rearward. This reduction in drive torque on the front axle ultimately reduces the torque steer effects experienced. However, it also reduces the overall efficiency of the vehicle as the front drive unit is more efficient than the rear drive unit. Furthermore, the performance of the vehicle drops as well, as it is constrained by the power the battery pack can deliver and not the maximum power output of the motors. Therefore, by biasing more towards the rear less electrical energy can be converted into kinetic energy.

1.2 Objectives

The objective of this project is to develop a Simulink model which can be used to analyse torque steer. This model should allow investigation into the root causes and investigate possible mitigation strategies. The mitigation strategies can either be applied to current vehicle by means of firmware updates or design change proposals, which can be taken into consideration when developing the next generation of vehicles. These objectives can be fulfilled by answering the following questions: "Can a model be used to analyse the root causes of torque steer?" and "How can torque steer be reduced or eliminated?".

To answer these questions a multi-body model of the vehicle will be developed which will aid in the analysis of the torque steer. Additionally, it will be used to explore the effectiveness of possible mitigation strategies. This model is tailored to the Model S which is the subject of this investigation. However, the model is easily adaptable through vehicle parameter alterations to represent other vehicles.

To limit the scope of the project only the front suspension is modelled in detail. The rear suspension will be simplified to having a single degree of freedom in the vertical axis. Furthermore, all components, except for the suspension bushings, are assumed to be infinitely stiff and any deflections are, therefore, omitted from the model. Any effects from road conditions are also omitted and the model assumes a perfectly flat road plane.

1.3 Contributions

The main contribution of this research is the multi-body model which can be used to analyse and simulate torque steer on any vehicle. The model allows to visualise the impact of design changes on torque steer. Moreover, it allows enabling and disabling of subsystems to isolate the effects of a specific component.

Additionally, the root cause of torque steer on the all-wheel drive Tesla Model S has been found and

mitigation strategies for the torque steer behaviour are proposed. The first strategy is a hardware redesign dedicated to the next generation of vehicles and the second strategy is a firmware change which serves the vehicles already delivered or currently in production.

1.4 Thesis Outline

Chapter two will give an overview of the possible root causes of torque steer, which have been discussed in literature. This includes the effects of asymmetric tractive forces, suspension geometry and power train specifications. This chapter also presents the known mitigation strategies already explored to reduce torque steer. This includes both passive and active solutions in the form of suspension modifications and power steering control respectively.

Chapter three presents the developed torque steer analysis tool. This includes the modelling and integration of each subsystem and the validation of the full vehicle model.

The fourth chapter discusses the results of the simulation study. It includes the simulations performed using the developed tool, which highlights the effects and contribution of each subsystem with respect to torque steer. Furthermore, mitigation strategies explored both in the model and on an actual vehicle are presented here.

Lastly, the final chapter discusses the recommendations for potential further research. The research shows that a few components behaved unexpectedly. This could not be further researched due to time and facility constraints. Hence, there are still some questions regarding torque steer on the vehicle left unanswered.

2 Literature Review

2.1 Root Causes of Torque Steer

Torque steer has been a known phenomenon for quite some time and extensive research into it has already been conducted. This subsection will discuss various root causes and mitigation strategies.

Tractive forces

Even when ignoring the suspension geometry, a form of torque steer can arise due to different tractive forces at left and right side of the vehicle [1], [2]. This can occur when the vehicle encounters a mu-split scenario where one wheel has significantly less traction than the other. As depicted in Figure 2.1 the imbalance in forces creates a yaw moment around the centre of rotation of the vehicle. This could be interpreted as torque steer as it will result in the vehicle veering from a straight line.

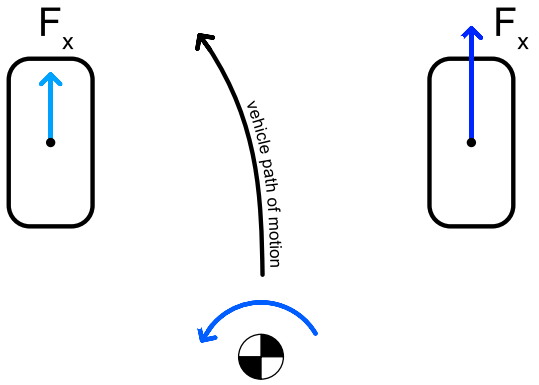

Figure 2.1: Differing tractive forces resulting in a yaw moment

Wheel Centre Offset

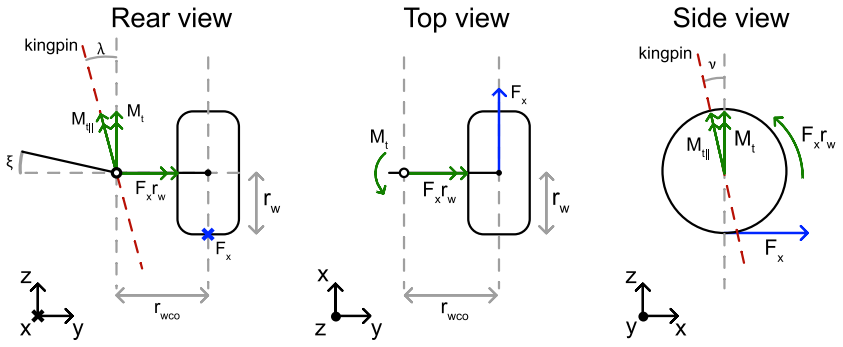

Figure 2.2: Suspension geometry parameters and kingpin moment due to the tractive force [3].

The entire hub assembly rotates around the kingpin axis. The wheel centre offset, r_{wco}, is defined as the orthogonal distance between the centre of this axis and the centre of the wheel as depicted in Figure 2.2. The tractive force acting at the tire contact patch will generate a moment around the kingpin axis due to this leveraging arm, as given by the relation [4] [5]

$$M_t = F_x r_{wco}, \tag{2.1}$$

where M_t is the moment around the kingpin and F_x is the tractive force. This moment then needs to be projected onto the kingpin axis to obtain the contribution to the steering torque. The relation between the aforementioned moment and the projected moment is given by [4] [5]

$$M_{t||} = M_t \cos(\nu)\cos(\lambda). \tag{2.2}$$

Here $M_{t||}$ is the projected moment around the kingpin axis due to the tractive force, ν is the caster angle and λ is the kingpin angle. The left- and righthand side moments will cancel each other if the suspension geometry is symmetrical and assuming that the tractive forces are the same. If for any reason the left and right wheel centre offsets or the tractive forces deviate from one another the kingpin moments will be different. These moments will generate a force on the steering rack trough the tie rods. If there is a difference in these moments there will also be a difference in forces exerted on the steering system. The resultant force on the steering system can be felt in the steering wheel and will tend to steer the vehicle to the side with largest tractive force.

Secondary CV joint moment

In many front wheel driven vehicles the drive shafts are not symmetrical for packaging reasons. Due to this the drive shafts have different inclination angles as they need to cover the same vertical distance at differing horizontal lengths. To achieve this the driveshaft contains two CV joints. When this joint is transferring a torque from one part of the shaft to another it will experience a secondary moment along the plane bisecting the joint, as depicted in Figure 2.3 [1]. This secondary moment will produce a steering moment around the kingpin axis. The relationship for this secondary moment is derived in [4] [5] and is given by

$$\vec{M_{cv2nd}} = F_x r_w(\cos(\xi) - 1)\vec{i} + F_x r_w \sin(\xi)\vec{j}, \tag{2.3}$$

where $\vec{M_{cv2nd}}$ is the moment vector due to the secondary torque in the CV joint, r_w is the wheel radius and ξ is the half shaft inclination angle, $\vec{i}$ and $\vec{j}$ are the horizontal and vertical unit vectors as depicted in Figure 2.3.

This moment is projected onto the kingpin axis by taking the dot product of $\vec{M_{cv}}$ and the unit vector of the kingpin axis [4] [5]. The kingpin axis is inclined by the kingpin angle λ giving the following relation for its unit vector

$$\vec{u_{kp}} = \sin(\lambda)\vec{i} + \cos(\lambda)\vec{j}. \tag{2.4}$$

$\vec{M_{cv2nd}}$ can then be projected onto the kingpin axis using this unit vector giving the relationship

$$\vec{M_{cv2nd||}} = \vec{M_{cv2nd}} \cdot \vec{u_{kp}} = F_x r_w \sin(\lambda)(\cos(\xi) - 1)\vec{i} + F_x r_w \cos(\lambda)\sin(\xi)\vec{j}. \tag{2.5}$$

Here $\vec{M_{cv2nd||}}$ is the secondary torque produced moment projected onto the kingpin axis. The magnitude of this projected moment is then defined by

$$|\vec{M_{cv2nd||}}| = F_x r_w \sqrt{\sin(\lambda)^2(\cos(\xi)^2 + 1 - 2\cos(\xi)) + \cos(\lambda)^2 \sin(\xi)^2}. \tag{2.6}$$

Equations (2.2) and (2.6) show that moment on hub around the kingpin axis is a function of the tractive force, tire radius, wheel centre offset, kingpin angle, caster, and the inclination of the half shaft.

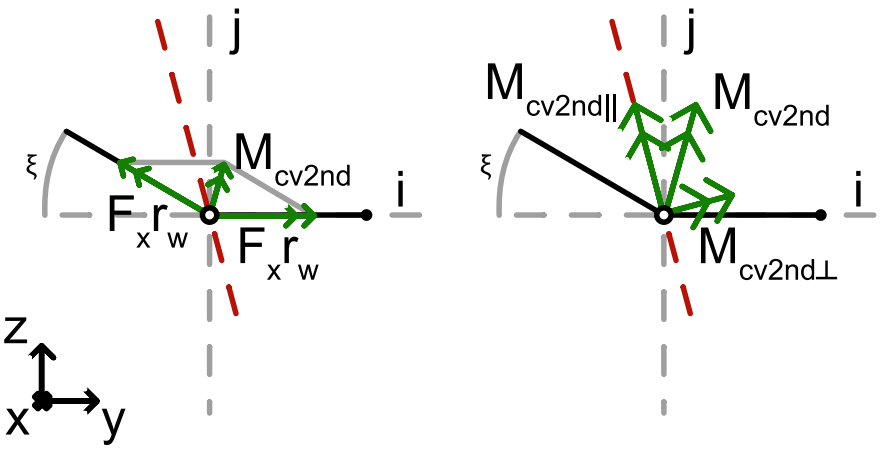

Figure 2.3: The secondary torque produced by the CV joint [4] [5].

Powertrain Roll Axis

It is possible that no difference in half shaft inclination is observed over the entire range of suspension travel. Nevertheless, a difference in shaft angle may still present itself when accelerating. A reactive torque will be exerted on the motor when a torque is applied to the wheel via the driveshafts. The motor will roll due to this torque and the compliance in the engine mounts. This axis about which it rolls is usually designed to be diagonal due to NVH concerns as depicted in Figure 2.4 [1] [6]. This is done in an attempt to decouple the vibration caused by the powertrain from the chassis.

As the power train rolls backwards the inner CV joints move forward and upwards. As the distance to the roll axis differs from left to right the displacement differs as well. This results in one side of the differential output rising more than the other resulting in a deviation in half shaft angle under aggressive acceleration.

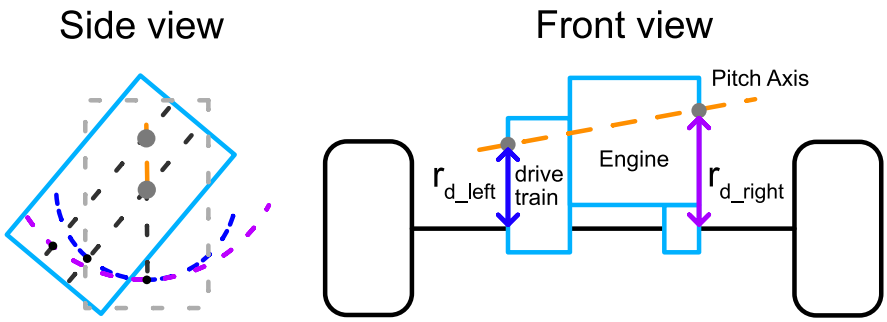

Figure 2.4: Driveshaft inclination deviation as a result of a diagonal powertrain roll axis [6].

Evidently, torque steer will only be present at high torque due to motor rolling as (2.6) shows that the inclination angle influences the moment around the kingpin generated by the CV joint. A deviation in half shaft inclination angle would lead to a deviation in M_{cv2nd}.

Differential

Most passenger vehicles are equipped with an open differential. This differential makes sure that the two connected wheels can rotate at different speeds and provides an equal amount of torque to both of them at all times.

This, however, applies to an ideal open differential. In reality a differential has some internal resistance, which results in it providing more torque to the slower wheel [7]. Moreover, it may deform when significant amount of torque is applied to the differential and the planetary gears could start to bind adding to the unequal split of output torque [8] .

A deviation in differential output torque would result in different tractive forces which is a parameter in both (2.2) and (2.6). Additionally, as discussed earlier, the different tractive forces left and right will also generate a yaw moment.

Load Distribution

The normal force on a wheel has a significant impact on the available tractive force defined by [2]

$$F_x = \mu F_z, \tag{2.7}$$

where μ is the coefficient of friction and F_z is the normal force on the tire. A variation in the coefficient of friction has already been discussed, but a dissimilar vertical wheel force distribution could result in the same behaviour [6].

Driveshaft Stiffness

Due to packaging reasons the left and right half shaft often have different lengths. Therefore, the shafts will also have a different torsional stiffness if not accounted for [6]. This should only be noticeable in transients. The deviation in deflection will result in a phase difference in the output torque of the shafts [9]. An imbalance in tractive force can be observed in transients events due to this.

2.2 Torque Steer Reduction

Ford developed their Revo knuckle suspension to reduce torque steer [10]. The objective is to reduce the wheel centre offset of a traditional McPherson suspension used on many front wheel driven vehicles. As discussed the wheel centre offset determines the moment around the kingpin axis resulting from a tractive force. If the wheel centre offset were to be smaller, the moments would be smaller and thus any difference between left and right due to varying tractive forces would be reduced as well, thus alleviating torque steer.

The reduction in wheel centre offset has been achieved by splitting the strut into two parts, the spring-damper assembly and a steering knuckle as depicted in Figure 2.5. In doing so the axis about which the knuckle rotates has been moved closer to the wheel centre, thus reducing the wheel centre offset.

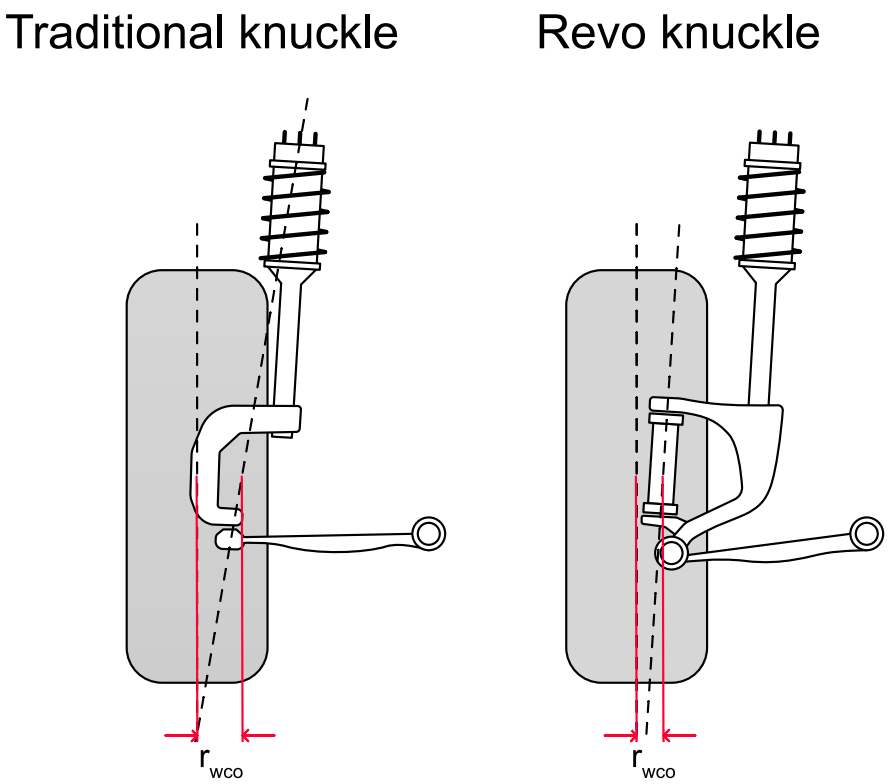

Figure 2.5: The Revo knuckle design [11].

Active control strategies can also be used to counteract torque steer. Electric power-assisted steering systems (EPAS) have been widely adopted for about a decade now. Torque steer compensation using the EPAS has been attempted. J. Dornhege conducted research for the Ford Motor Company in [12] and [13]. In these papers the forces on the steering rack due to torque steer are estimated using observers and using the data acquisition systems already present on passenger vehicles. These systems include but are not limited to the ESP to estimate vehicle dynamics and the EPAS itself. The direction and magnitude of the force are calculated using the model. This additional force is applied as an overlay on top of the normal power steering support requested. It has been shown that this approach can compensate for torque steer on dry and flat surfaces.

Additionally, H. Gökhan [14] also conducted a study into finding a mitigation to torque steer using the electric power steering system. In the paper a similar approach to controlling the EPAS is taken. Here the forces resulting in torque steer are modelled as well. Using this model and already available sensors the required compensating torque is computed. It noted that a significant fraction of the forces on the steering system are a result of the desired self aligning torque created by the tires, the remainder is mainly caused differing secondary couples.

3 Torque Steer Analysis Tool

A multi-body model has been developed to analyse the torque steer observed in the Tesla Model S. The model is based upon a previously developed multi-body model to analyse and design multi-link suspension systems [15]. This model was developed in MALTAB/Simulink using the Simscape multi-body library and can be used for vehicle dynamics analysis. In the original model, the chassis is fixed in space and the ground plane under each wheel has four degrees of freedom. The chassis has six degrees of freedom, as the deviation from an intended path is of interest in this investigation. Additional subsystems have been implemented. This includes springs and dampers, tires, the steering rack and a powertrain. Figure 3.1 presents the complete model, as visualised in Simscape.

The analysis tool can simulate the vehicle motions for a set of vehicle parameters and driver inputs. This is achieved using various modules. The first module handles the inputs for the model. It will load the predefined vehicle parameters and the driver inputs. The driver inputs can either be prescribed as a function of time or they can be loaded from a MoTeC measurement file to replicate performed manoeuvres. The second module, the Simulink model, uses this data to perform the actual simulation and visualisation. The last module post-processes the data collected during the simulation, prepares them for plotting and creates the figures. More details on the structure and the operation of the tool are presented in Appendix A.1. This section elaborates on the model itself and the vehicle subsystems implemented.

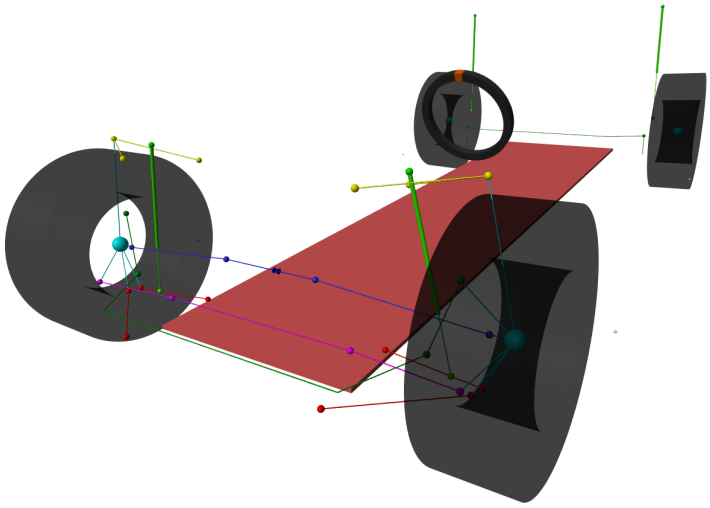

Figure 3.1: The Simscape torque steer simulation model visualised

3.1 Model Development Approach

As stated before, the model is based on previous work and requires modifications and extensions. Each subsystem will be modelled in its own environment first. Here it will be refined and validated using available measurement data, before integrating it into the full vehicle model. Doing this will save significant development time as the full model will grow in complex quickly and will thus take more computation time. Additionally, the inputs and outputs can be defined to eliminate the influence of other components in the full vehicle model. After the subsystem has been validated on a subsystem level it can be integrated into the full vehicle model. Once integrated the subsystem will be validated again to verify that it still behaves as expected when interacting with the full vehicle.

3.2 Vehicle Data

Throughout the development of the actual vehicle, a lot of parameters have been documented and validation data has been recorded. Many subsystems have been validated both on a subsystem level and on a vehicle level. The data gathered during this phase has been used to create models of the subsystems of interest. CAD drawings are used to obtain hardpoints locations and dimensions of various components required to model the suspension. Furthermore, various design specification documents have been used to obtain parameters for components which include but are not limited to the springs, dampers, steering rack and bushings. Magic Formula parameters of a tire are also required. The recommended tires had been parameterised for the internal vehicle dynamics simulation and these were made available to be used for this research.

Also available is the measurement data gathered during vehicle validation tests. These tests included wide open throttle acceleration, 1g deceleration and various steering manoeuvres. For these tests, a Model S was fitted with a variety of sensors as listed in Table 3.1. Additionally, CAN traffic is included in the measurement data. This provides all signals required to reproduce a vehicle validation test in the model and to compare the results directly to what has been measured.

Table 3.1: Vehicle equipped instrumentation

Instrument	Signals
Inertial measurement unit	a_x, a_y, a_z
Gyroscope	roll rate, pitch rate, yaw rate
Body mounted ride height lasers	all four corner ride heights
GPS	vehicle position, heading and velocity
Wheel force transducers	F_x, F_y, F_z, M_x, M_y and M_z of all four tires
Wheel vector sensors	camber and steering angle of front tires
Tie rod strain gauges	Tie rod forces

Besides validation data, drive unit dynamometer data has also been collected. This test was performed to look into the differential behaviour under load, as it was suspected to bias torque. During the test, the drive unit itself was placed onto a dedicated dynamometer. Here the motor speed and torque and the axle speed delta were set while both output shafts torques were measured.

3.3 Suspension and Tires

The provided model was adapted to the suspension of the Model S, which was done through the included parametrisation of all components. Slight modifications had to be made to the struts as the Model S does not have a pushrod spring-damper system. Instead it is equipped with a conventional strut connected to the body and the aft link. A schematic representation of the revised front suspension is depicted in Figure 3.2. The suspension of the front left corner of the vehicle is presented in Figure 3.3. The rear suspension has been kept simple to reduce complexity and computation time. This can be done as its direct impact on the steering wheel torques is negligible. Although rear axle dynamics could contribute to undesirable path deviations, it has been assumed to be symmetrical and therefore insignificant as the forces on the left and right side of the vehicle cancel each other out.

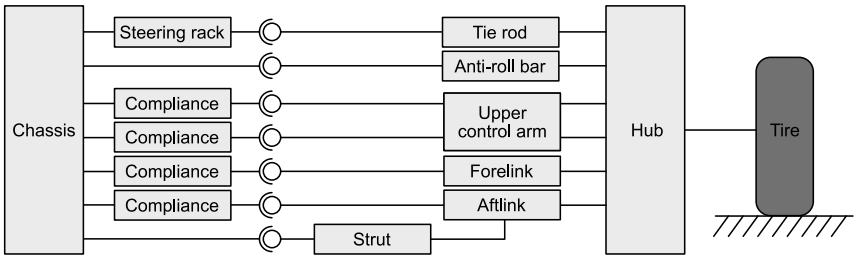

Figure 3.2: The schematic representation of the front suspension

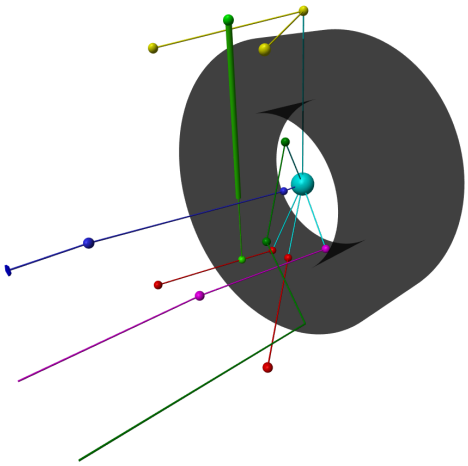

Figure 3.3: A close-up of the front suspension

With the alterations made the model can be used to review the kinematics of the suspension and verify them against design specifications. An important parameter here is the wheel centre offset of the front suspension. As depicted in Figure 3.4 the wheel centre offset of the right wheel increases as the steering wheel is turned to the left, while the left wheel centre offset decrease. Consequently, steering slightly to the left will cause an imbalance in kingpin moments, which may steer the vehicle further left creating a greater imbalance. The steering behaviour could therefore be unstable if other other forces do not stabilise it.

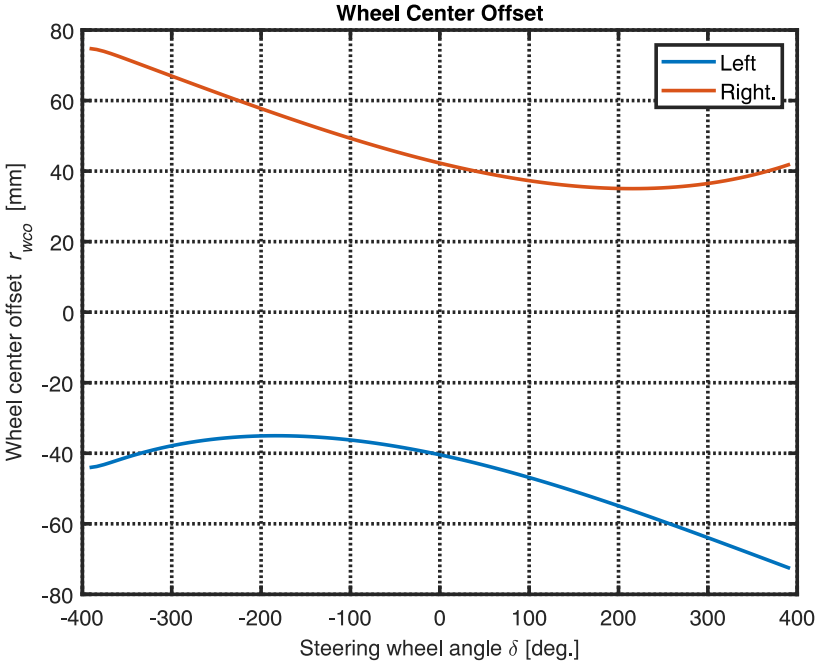

Figure 3.4: The modelled wheel centre offset over the steering wheel angle (Right is positive)

Additional rework has been done to convert fixed chassis, to a chassis which has six degrees of freedom. To achieve this the moving ground planes have been replaced with a fixed infinite ground plane. Additionally, a rear suspension needs to be modelled. The choice was made to reduce the complexity of the rear suspension to limit the simulation time of the model. This has been achieved by omitting all suspension components and restricting each rear hub to have a single degree of freedom along the vertical axis. The struts and the anti-roll bar have been integrated into the rear suspension as well to still be able to properly capture the behaviour of the actual vehicle.

Compliance of the suspension bushings has been added to front suspension in the model. Ideally, this would be done by modelling a spring force in two directions at the inner hard point to reflect the axial and radial deflections. However, due to computational performance constraints, this was not possible. Therefore, it was opted to only simulate the radial deflection in line with the suspension link itself. This approximation holds for all but the aft link, as they only serve to keep the hub in position and thus only transmit forces in the radial direction. As the strut is connected to the aft link it will also generate a moment which causes a downward force on the bushing. As this deflection is quite constant it has been omitted from the model.

The anti-roll bar has been modelled through infinitely stiff rods representing the actual shape. In the centre where the two halves connect a torsional spring has been included, which has an equivalent stiffness compared to the actual anti-roll bar. This approach has been used for both the front and rear anti-roll bars.

The implementation of the tires has been achieved through the *Magic Formula Tire Force and Torque* Simulink block. This block implements the combined slip steady-state Magic Formula and uses this model to compute the various tire forces and torque. The block outputs relevant signals related to the tire itself. The inputs to the block are the parameters for the Magic Formula equations. The block itself is connected to the hub and the road plane

The validation of the complete vehicle model is done by replicating a performed manoeuvre. This manoeuvre consists of a wide open throttle acceleration, 1G deceleration, a right-hand hairpin corner and a final wide open throttle acceleration. The throttle, brake and steering inputs are presented in Figure 3.5. The path is presented in Figure 3.6.

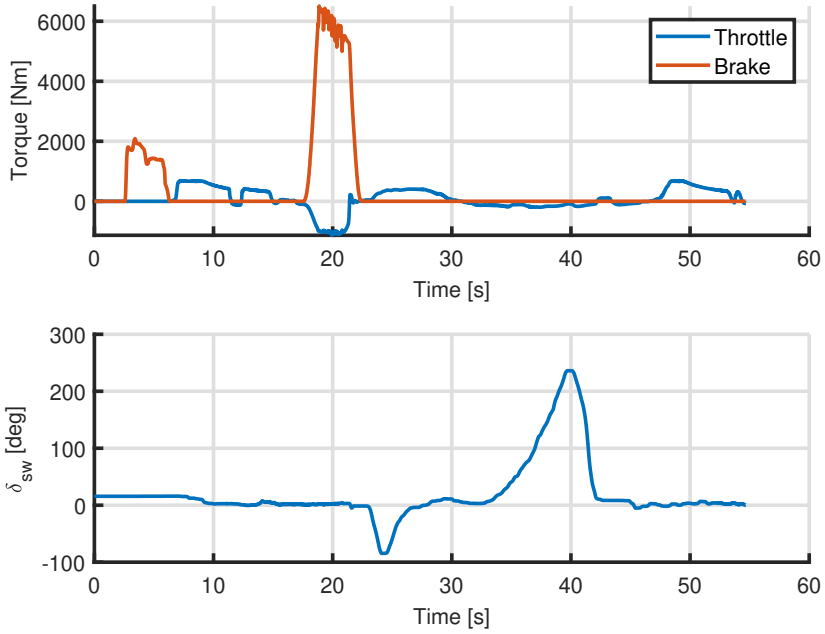

Figure 3.5: The driver inputs recorded during vehicle validation tests

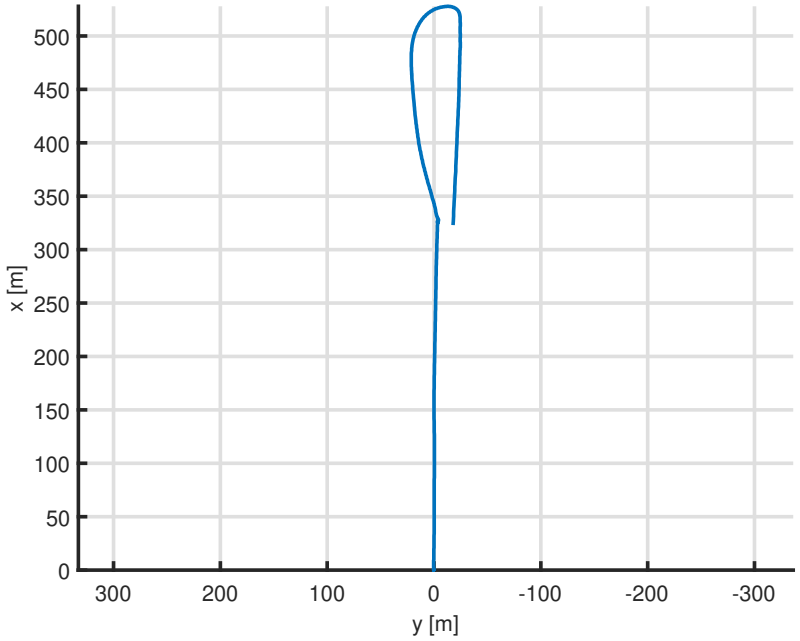

Figure 3.6: The path driven during vehicle validation

The vehicle accelerations and yaw rate are presented in Figure 3.7. In this figure and for all following figures the opaque lines represent the model, while the faded line represents the measurement data unless mentioned otherwise. The accelerations and yaw rate match the measurements closely except for the lateral acceleration, which is higher during the hairpin corner. This is likely due to the tires

generating slightly larger lateral forces. Nevertheless, the trajectory driven by the vehicle does not exactly resemble the original trajectory as shown in Figure 3.9. This is expected to be caused by small errors in the generated forces, which are integrated over time into sizeable errors. Furthermore, the model has a tendency to wander off to the right in comparison to the real vehicle. This could be due to many of the suspected contributors to torque steer, which tends to steer the vehicle to the left, not being implemented yet.

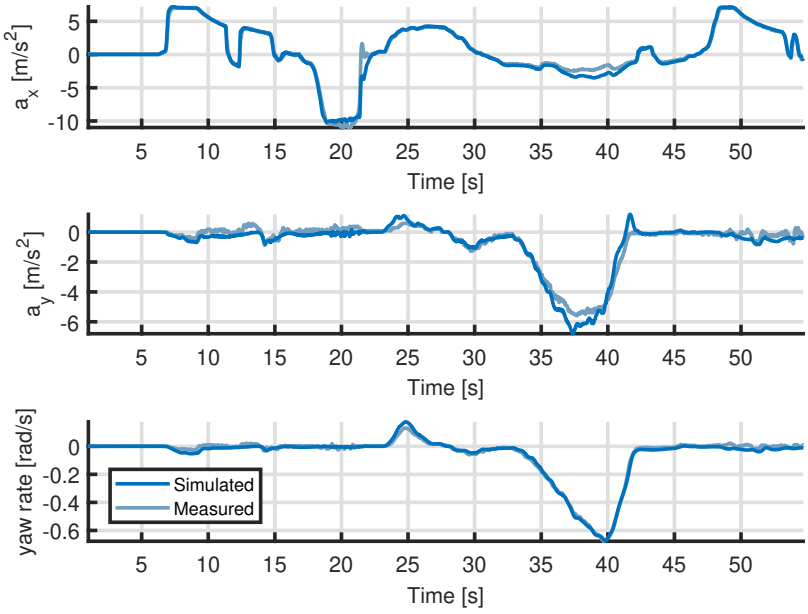

Figure 3.7: The acceleration and yaw rate of the vehicle

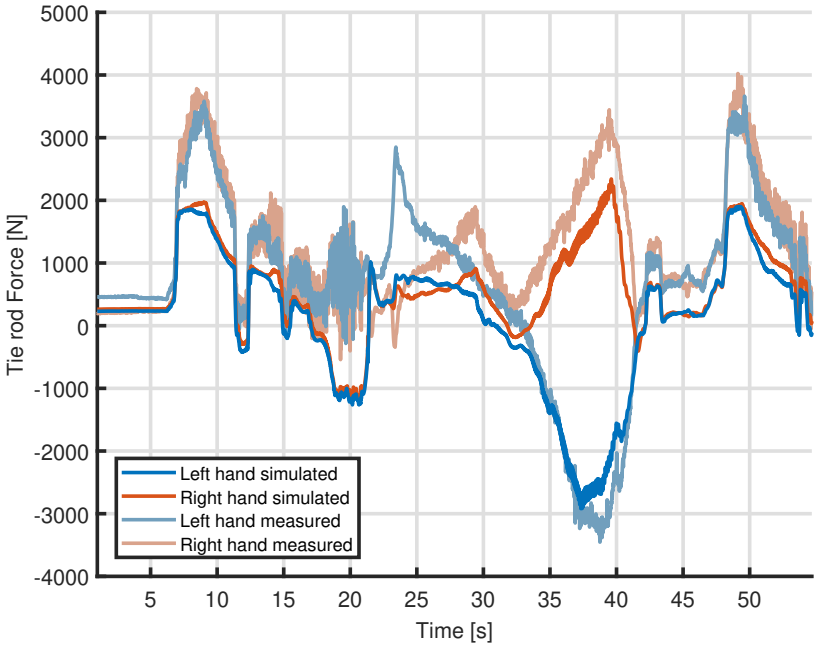

Figure 3.8: The tie rod forces of the vehicle

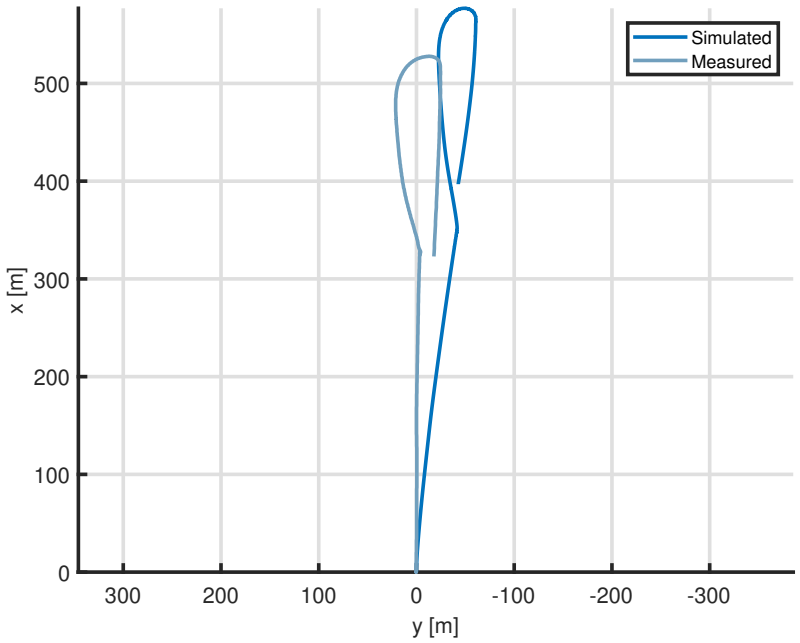

Figure 3.9: The trajectory of the vehicle

The relevant tire forces and moments are presented in Figure 3.10. As presented in Figure 3.10a the tractive forces of the left and right tire do not exactly match the measured tractive forces. Instead the modelled forces are an average of the measured tractive forces. This is expected as the model splits the produced motor torque evenly to both tires. The only difference observed here is a slightly

lower magnitude in braking force which would be down to the ABS in the model reducing braking forces more than it would on the actual vehicle.

The weight transfer of the vehicle is replicated well as highlighted in Figure 3.10b. The only anomaly observed here is the static weight distribution not matching that of the test vehicle. This is due to the effects of the higher rear left air spring pressure not being implemented yet.

The lateral forces generated by the front tires replicate the forces seen in the measurement data as depicted in Figure 3.10c. The rear tires, however, do not. This is expected to be caused by the simplifications made to the rear suspension. Due to this, no toe gain is induced, which has a significant impact on the slip angle and thus also the lateral forces generated. This is especially evident when braking where the rear tire in reality generates a lateral force close to 1 kN while the model generates barely any lateral force.

The self-aligning moments similar same deficiencies as presented in Figure 3.10d. The simulation results of the rear tires suffer from not having a suspension model. The front tires match the expected self-aligning moment during acceleration, while the rear tires generate too little. In this simulation, the front tires generate too little self-alignment while braking as well. Whereas the measurements reach a self-aligning moment of 200 Nm the model only generates moments up to 100 Nm.

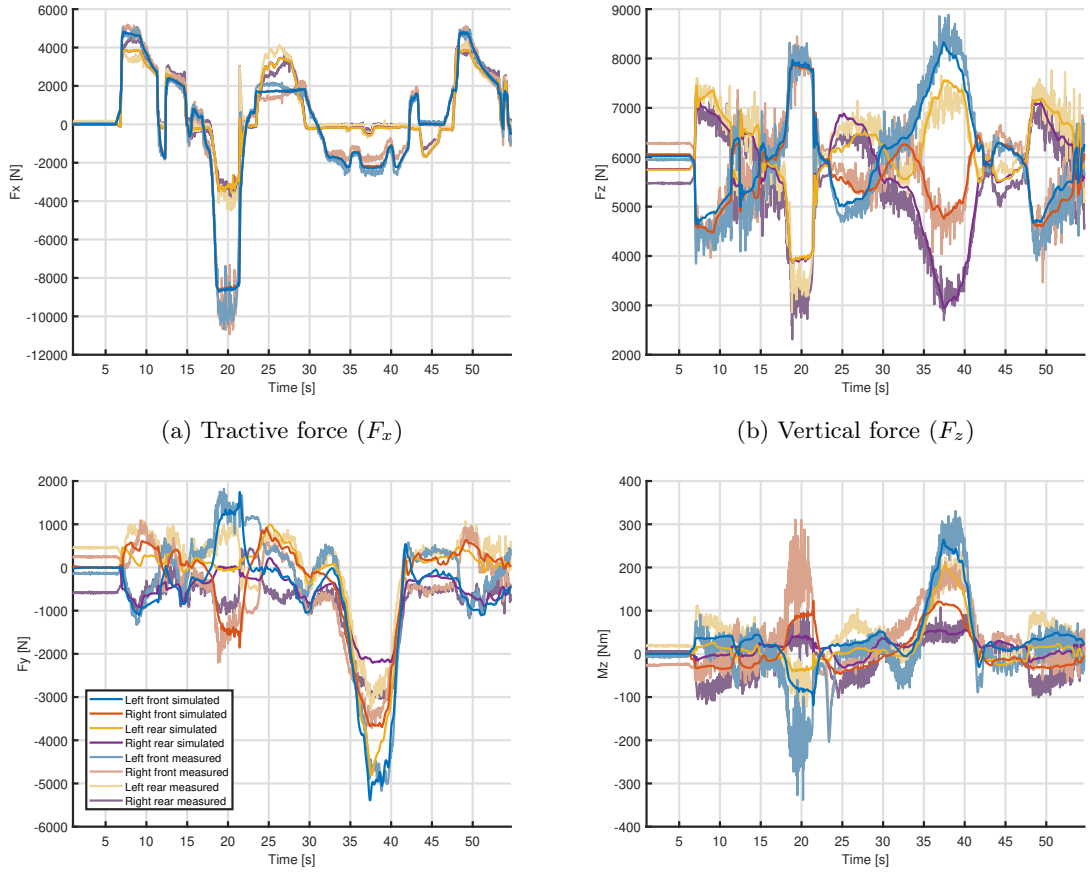

(a) Tractive force (F_x)

(b) Vertical force (F_z)

(c) Lateral force (F_y)

(d) Self aligning moment (M_z)

Figure 3.10: The tire force validation

3.4 Springs and Dampers

The actual vehicle contains air springs. To reduce the model complexity the measured spring rate of the air spring is used to find the spring forces. This omits the modelling of any pressure and air volume alterations.

An anomaly found is that the pressures in the air suspension are asymmetrical. When levelling the vehicle to a specific ride height the front right, rear left or both air springs will have a higher pressure compared to the front left and rear right air spring pressures. This was confirmed to occur on multiple vehicles by running a measure air spring pressure service routine. The results of this routine are presented in Table 3.2. The consequence of these pressures was visible in the four tires vertical forces measured. Here a high load on the front right and rear left was noticed compared to their respective counterparts.

Table 3.2: The measured pressures in the air springs

Vehicle	Air suspension system	Pressures [Bar]	
2018 Refresh Model S	Tesla air suspension	8.1	8.1
		6.0	5.7
2019 Refresh Model S	adaptive Tesla air suspension	8.1	8.1
		5.7	5.2
2022 Palladium Model S	adaptive Tesla air suspension	7.4	7.6
		5.4	5.4
2022 Palladium Model X	adaptive Tesla air suspension	8.2	8.7
		6.5	6.2

The spring rate has to be made dependant on the air spring pressure to capture this in the model. The force produced by a pressure on a surface and thus the force the strut will exert is given by

$$F_s = (p - p_b)A, \tag{3.1}$$

where F_s is the force, p is the pressure inside the strut, p_b is the atmospheric pressure and A is the area of the surface. The pressure, volume and area, however, vary continuously during jounce and rebound. The volume and surface area are dependent on the design and spring travel. The new internal pressure can be found through the adiabatic process as no significant amount of heat is generated and the air mass remains constant. The equation for an ideal gas undergoing an adiabatic process is given by

$$pV^n = constant \tag{3.2}$$

where V is the air volume, n is the adiabatic index. Substituting (3.2) into (3.1) yields the following relationship for the force exerted by the air spring

$$F_s = \left(p_0 \left(\frac{V_0}{V_1}\right)^n - p_b\right) A(x), \tag{3.3}$$

where p_0 is the initial pressure reached when levelling the vehicle, V_0 is the initial volume, V_1 is the new volume as a result of jounce or rebound and x is the strut travel.

The assumption has been made that an increase in initial pressure will increase the spring rate with the same factor as modelling air springs was outside of the time frame of this project. This assumption can be made as an increase of the initial pressure does not have a significant influence on the ride height, hence $A(x)$ will remain the same. Additionally, p_b has been ignored as its influence is significantly smaller compared to the internal pressure. Therefore, the spring rate can be increased linearly to reasonably approximate an increased initial pressure.

The non-linear damper characteristics are based on the actual measurements done of the damping forces for various speeds. These values have been modified slightly to match the rate of change seen during vehicle accelerations.

The validation of the springs and dampers is done at the same time as the validation of the suspension itself. The results show that the ride height of the model and the measurements match closely during straight-line acceleration. During braking the ride height is about 5 mm lower than what was measured. During the right-hand hairpin the left ride heights match the measurements, however, the right-hand ride heights are considerably lower. This is also reflected in the body roll which deviates 0.35° from measurements. This deviation could be due to the simplification of the rear suspension, as the hub motion is limited to a single degree of freedom. However, it is more likely a deficiency in the approach taken to model the air springs. This could not be resolved due time constraints.

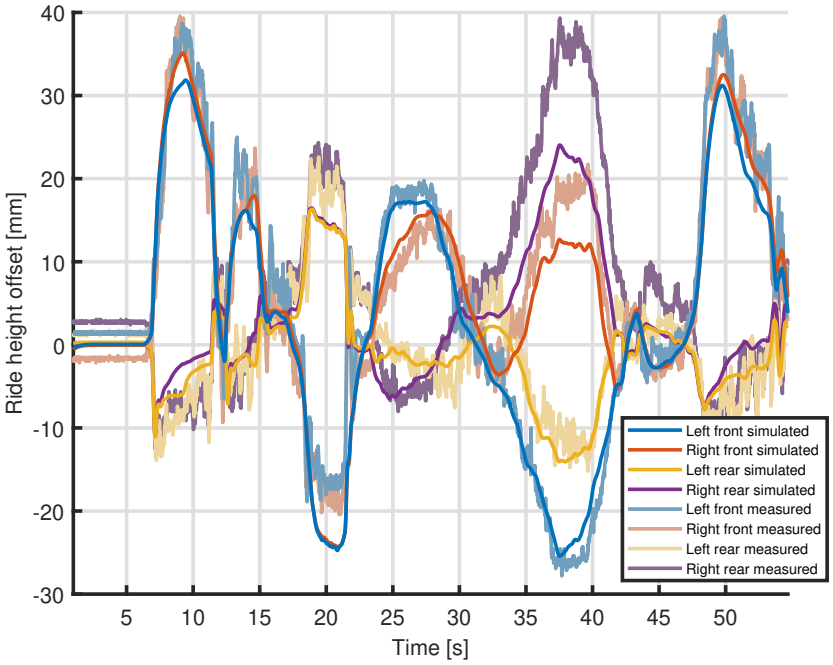

Figure 3.11: The ride height

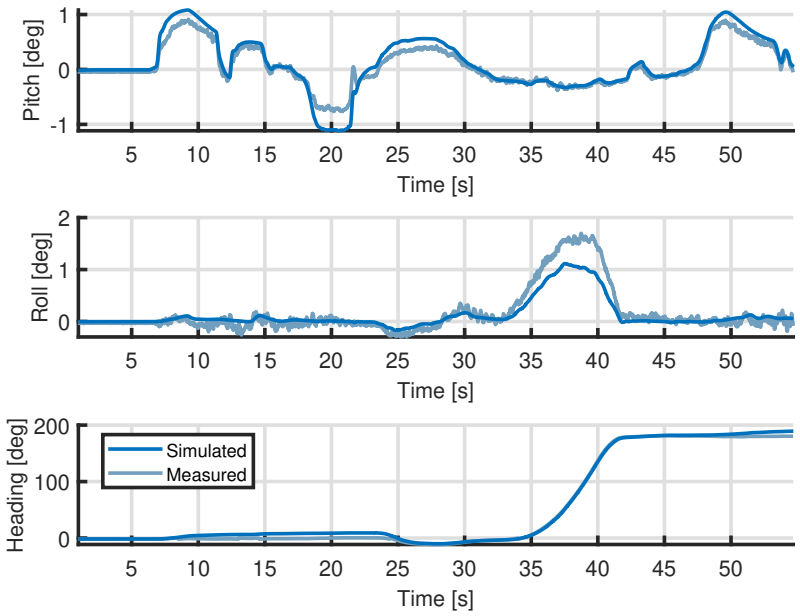

Figure 3.12: The vehicle body roll, pitch and heading

3.5 Steering System

The steering system has to be modelled to simulate the forces on the tie rods and the torque produced on the steering wheel caused by the torque steer. The basis of the steering system is the steering rack. The steering wheel is connected to the steering rack via a steering column and a rack and pinion combination. To assist the driver an electric assist motor will exert additional force on the rack trough a recirculating ball gearbox. A recirculating ball gearbox transforms rotary motion into a linear one similar to how an ordinary lead screw would. However, instead of threads interfacing with each other ball bearings are used, which greatly reduces friction. The amount of steering assist is based upon the the torque exerted on the steering column and the vehicle speed. The torque exerted on the steering column is determined by measuring the deflection of a torsion bar integrated into it.

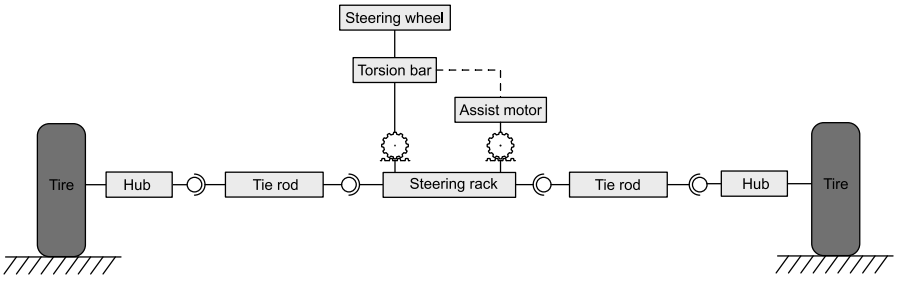

Figure 3.13: The schematic representation of the steering rack

The model of the steering rack is built up similar to the physical system. Figure 3.13 depicts the schematic representation. The steering wheel is connected through a torsion spring and a rack and pinion combination to the steering rack itself. The physical steering column is omitted however,

its mass and inertia have been lumped together with the steering wheel. Another deviation from reality can be found in the steering assist motor. Instead of implementing a full recirculating ball gearbox, it has been simplified to a rack and pinion combination with the same effective gear ratio. The relationship between the screw lead and the radius of the pinion is given by

$$r_{pinion} = \frac{L_{EPAS}}{2\pi\gamma_{EPAS}}, \tag{3.4}$$

where r_{pinion} is the radius of the pinion, L_{EPAS} is the screw lead and γ_{EPAS} is the gear ratio of the gearbox of the electric power-assisted steering motor. Lastly, a coulomb friction force has been included on the rack. To improve the performance of the simulation the discontinuous sign operation has been replaced by a hyperbolic tangent function, which provides a continuous approximation of the sign function.

The steering subsystem is also in need of a model representing a human interacting with the steering wheel as it would otherwise be kept perfectly straight. This has been achieved by implementing a PID controller, which tracks the reference steering wheel angle and exerts a torque on the steering wheel. The output of the PID controller can be set to zero to simulate a human driving without his hands on the steering wheel. An additional mode which directly controls the position of the rack, is available in case measured rack displacements are used as input.

The steering system is first modelled in a separate environment to exclude any inaccuracies already introduced into the model. To validate the model the steering wheel angle and torque have been used as input. Additionally, the tie rod forces measured are used to substitute the tie rods themselves. The driver model can track the reference steering wheel angle, δ_{sw}, with an average steering wheel angle error of 4° as depicted in Figure 3.14. The torsion bar torque, T_{sw}, required to track this reference, matches closely with the measurements.

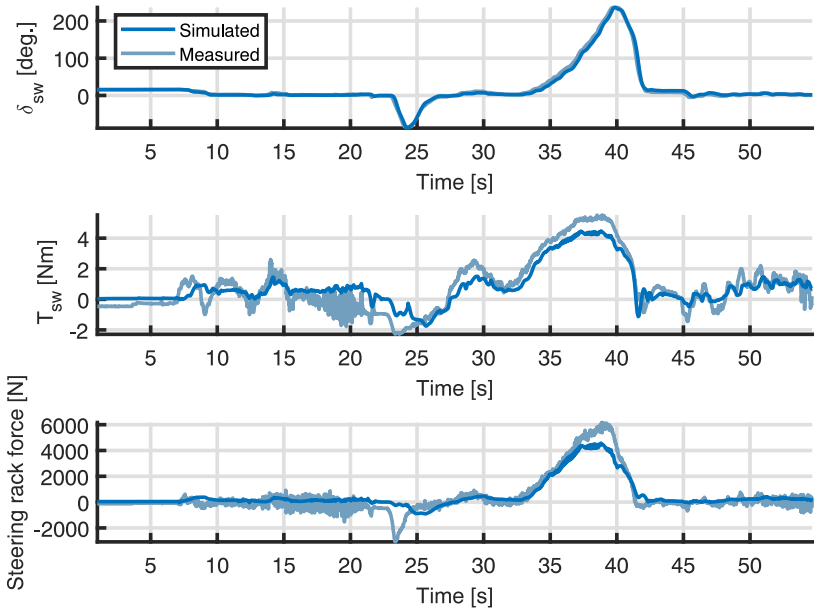

Figure 3.14: The subsystem validation of the steering rack

The human driver PID controller was tuned to a step response to a steering angle of 100°. The controller parameters are listed in Table 3.3. The response of the controller contains an overshoot of 45.3° which is quite significant. However, as a step in steering wheel angle input rarely occurs

this does not pose a problem for this application. After the overshoot the controller requires 1.3 s to reach a steady state. The step response of the controller is presented in Figure 3.15.

Table 3.3: The human driver steering controller parameters

Parameter	Value
P	0.3
I	0.03
D	0.001

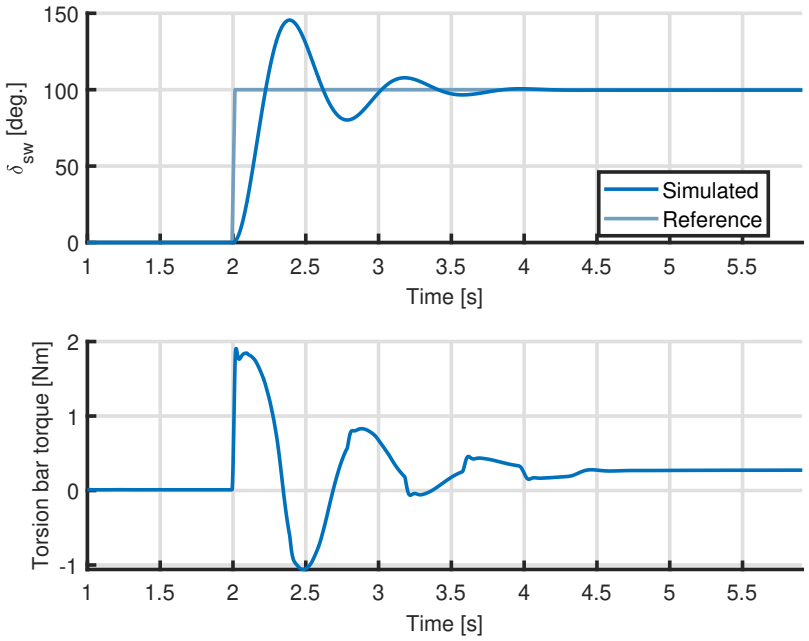

Figure 3.15: The step response of the human driver steering controller

After implemented it into the vehicle the same manoeuvre is used to validate the steering rack. During the simulation the human driver controls the torque on the steering wheel to track the steering wheel angle reference. As presented in Figure 3.16 the driver model is able to track the reference well, even with the additional disturbances from the suspension and tires. The torsion bar torque, although more noisy and a little less accurate, still resembles the measurement. The torque required to achieve the same steering wheel angle is about ten percent lower than it is for the actual vehicle. Lastly, the modelled rack forces generated closely resemble the measured signal except for a spike at around 23 s, as shown in Figure 3.17. Here stationary steering inputs results in significant forces on the steering rack, which the model does not replicate. Furthermore, the same reduction of the magnitude in torsion bar torque can be observed.

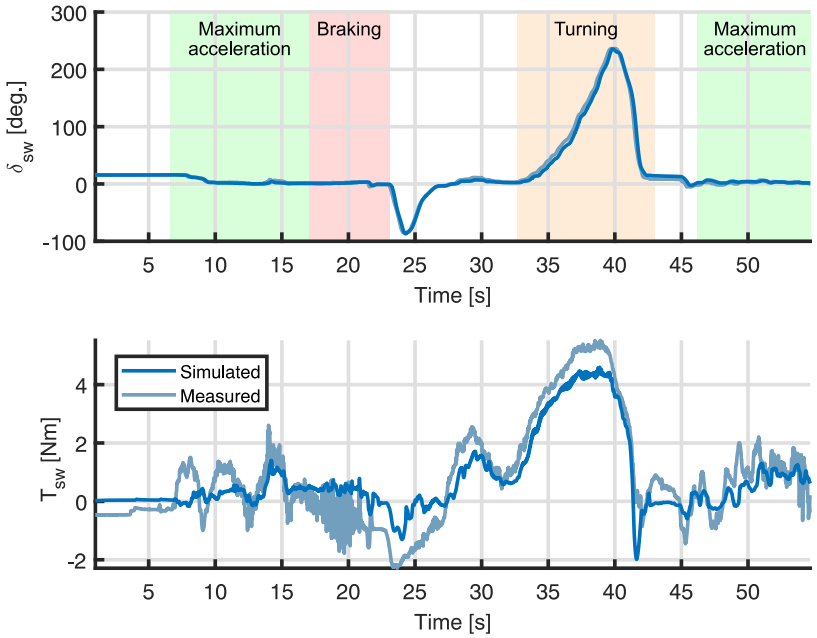

Figure 3.16: The steering inputs of implementation validation of the steering rack

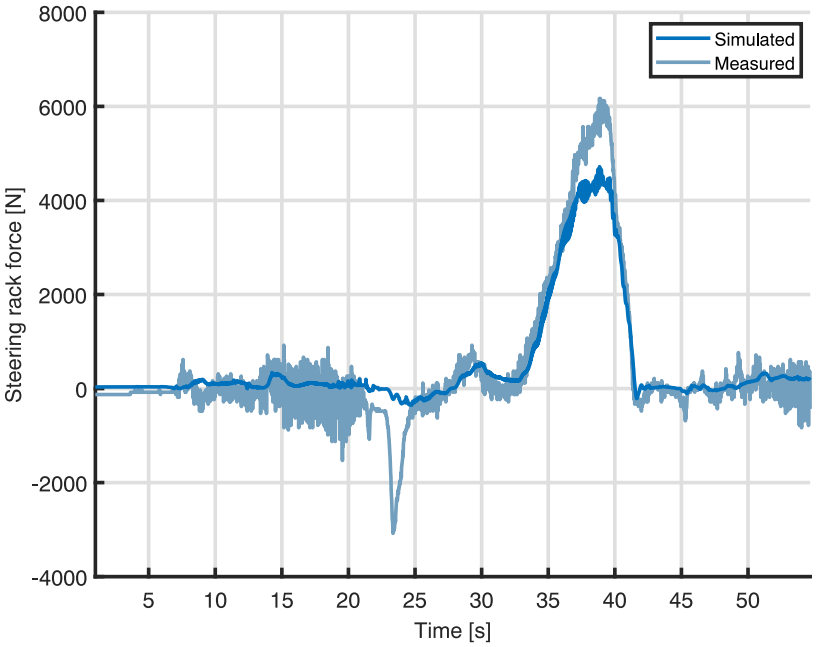

Figure 3.17: The implemented steering rack force

3.6 Motor Mounts

Previous investigations into torque steer revealed that the motor mount had an significant influence, thus it has been included into the model. There are three front motor mounts in Tesla Model S as depicted in Figure 3.18 indicated by the orange spheres. Two of the motor mounts support the right side, while a single mount supports the left side. The right side motor mounts are positioned higher than the left mount as evident is from Figure 3.18. The result of this is that the drive unit will not rotate purely about the y-axis under acceleration. This will result in differing bend angles for the two drive shafts.

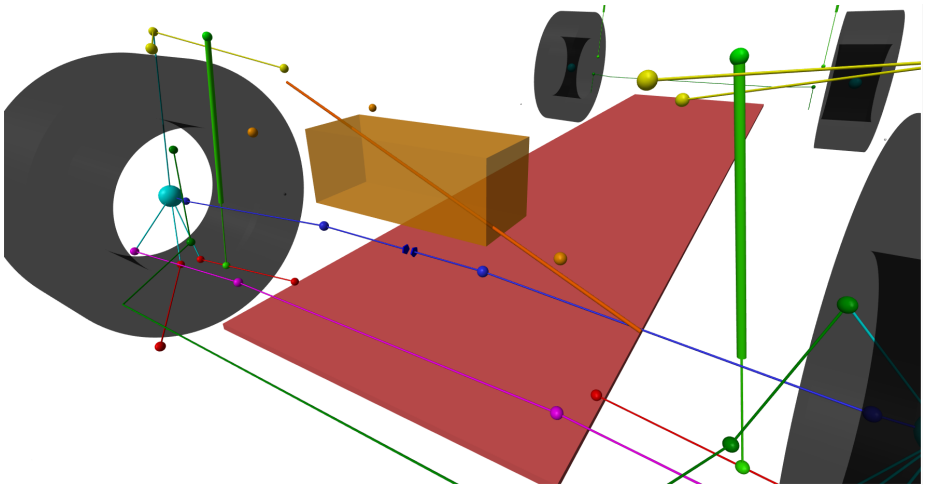

Figure 3.18: The approximation of the drive unit roll axis

A motor mounting system consisting of three deflecting rubber bushings cannot be implemented due to simulation performance limitations. An alternative approach is to approximate the axis about which the drive unit rolls. This reduces the system from six degrees of freedom to a single degree of freedom making it significantly easier to compute. The roll axis of the drive unit was approximated as the axis through the left mount and the centre of the right two mounts as depicted by the orange rod in Figure 3.18.

The model then refined by comparing the behaviour between the two methods in an environment separate from the vehicle. Here three bushings are positioned on the respective motor mount positions and a body is connected to them. A reactive torque is applied to drive unit and the rotation of both the rubber bushing model and the torque roll axis approximation is compared as depicted in Figure 3.19.

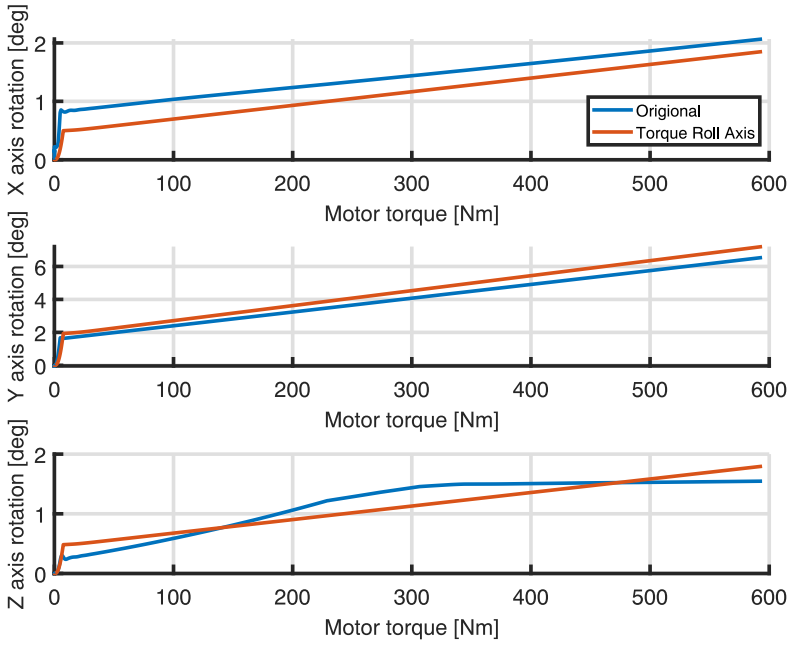

Figure 3.19: The validation of the motor mount model

The motor mount has been included in the vehicle after the validation. Figures 3.20a and 3.20b show the simulated deflection of the motor mounts during standstill and harsh acceleration respectively. Figures 3.20c and 3.20d depict the drive unit position in the actual vehicle during both standstill and harsh acceleration respectively. All figures present a front-view of the vehicle. The drive unit itself has been highlighted in the figures representing the actual vehicle.

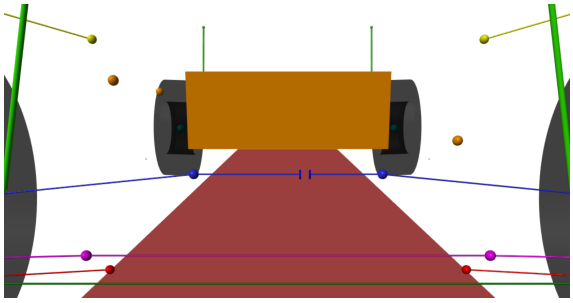

(a) Modelled drive unit position during standstill

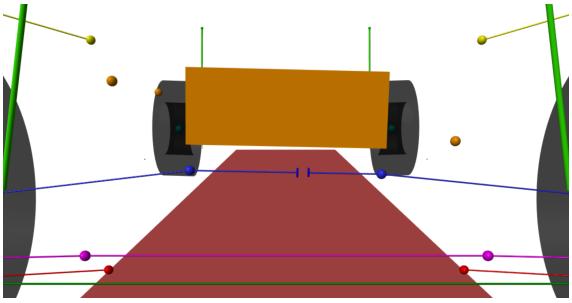

(b) Modelled drive unit position during acceleration

(c) Drive unit position during standstill

(d) Drive unit position during acceleration

Figure 3.20: The front-view of the drive unit positioning in the vehicle

The effect of the motor mount is clearly visible in the tie rod forces depicted in Figure 3.21. During the wide open throttle sections, at around 8 and 47 seconds, the right tie rod force is significantly higher than the left tie rod force. This was not present during the simulation of only the suspension and drive shafts. These forces result in a resultant force on the steering rack to the left.

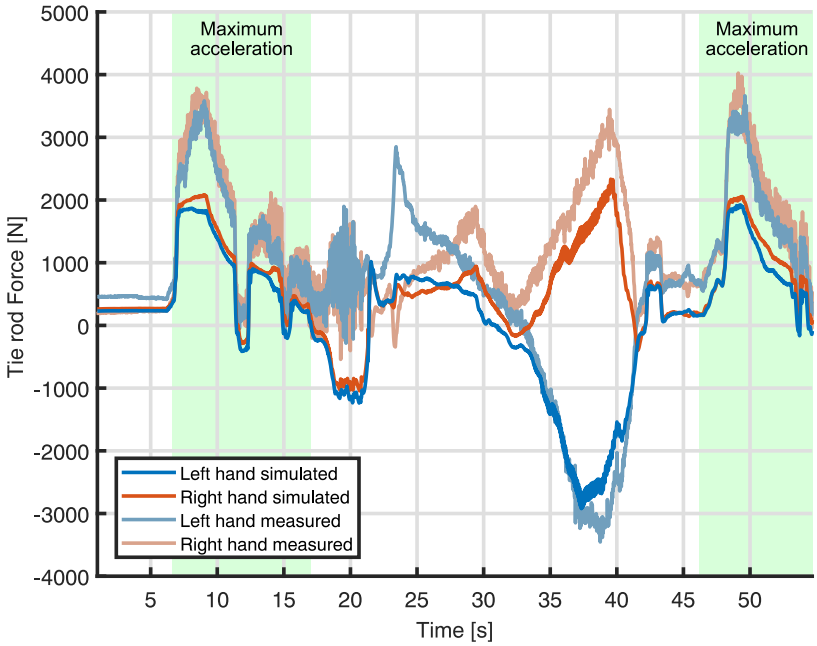

Figure 3.21: The tie rod forces influenced by the motor mount

3.7 Powertrain

To properly capture the behaviour of the powertrain the following elements need to be modelled: the motor itself, the gearbox, the differential, the half shafts, traction control and anti-lock brake system. The friction is omitted in all elements of the powertrain. The output torque of the motor is lowered slightly to match the tractive torques measured at the wheels, to represent the effect of friction in the drivetrain.

The torque output by the electric motor is modelled through the peak power output and the current angular velocity of the motor. Their relationship is given by

$$T_{em} = \frac{P_{peak}}{\omega_{em}}, \tag{3.5}$$

where T_{em} is the motor torque, P_{peak} is the peak power of the motor and ω_{em} is the angular velocity. The computed T_{em} is compared to the requested torque output of the motor and the smaller of the two is used. The requested torque is found by multiplying the peak torque output with the throttle pedal position to allow for power modulation.

The gearbox is represented by a gain. The torque output of the motor is increased by the gear ratio and applied to the differential. The angular velocity of the motor is given by the angular velocity of the differential multiplied by the gear ratio.

The peak output of the motor is often higher than the peak tractive force the tire can provide. Traction control needs to be implemented to limit the motor torque, otherwise larger spikes in wheel slip will be generated. This is achieved through a PID controller. The error for the traction controller is the amount the slip that surpasses the set limit as given by

$$e_\kappa = \begin{cases} 0 & \kappa < \kappa_{lim} \\ \kappa - \kappa_{lim} & \kappa \geq \kappa_{lim} \end{cases} \tag{3.6}$$

where e_κ is the error, κ is the largest of the left and right longitudinal wheel slip and κ_{lim} is the maximum longitudinal wheel slip allowed. The output of the controller is a reduction torque which is subtracted from the torque produced by the electric motor. This rudimentary traction control system is able to keep the wheel slip under the limit and is able to maintain traction during hard accelerations. The same system approach also used as an anti-lock brake system, where the brake torque is reduced based on the longitudinal wheel slip. One difference is that ABS can control an individual wheel compared to the TC system, which controls a drive unit thus influencing both left and right wheels at the same time.

Previous investigations into the differential include tests executed on a dynamometer. During the test the motor torque and speed were controlled. In addition the axle speed difference was controlled and the torque on both axles was observed. This was done for a variety of combinations of motor speed, motor torques and axle speed deltas.

From this data became evident that the torque bias produced by the differential is a function of the torque output by the motor and the axle speed delta amplitude. As presented in Figure 3.22, the applied torque dictates the maximum amplitude of the torque bias. Here it is also noted that the differential kept biasing torque after the shaft speed delta had been removed. This retained bias will only disappear after the motor torque is removed or if a reversed speed delta is applied. The speed delta influences the rise rate of the torque bias as shown in Figure 3.23. A larger speed delta will result in the torque bias reaching its peak value sooner.

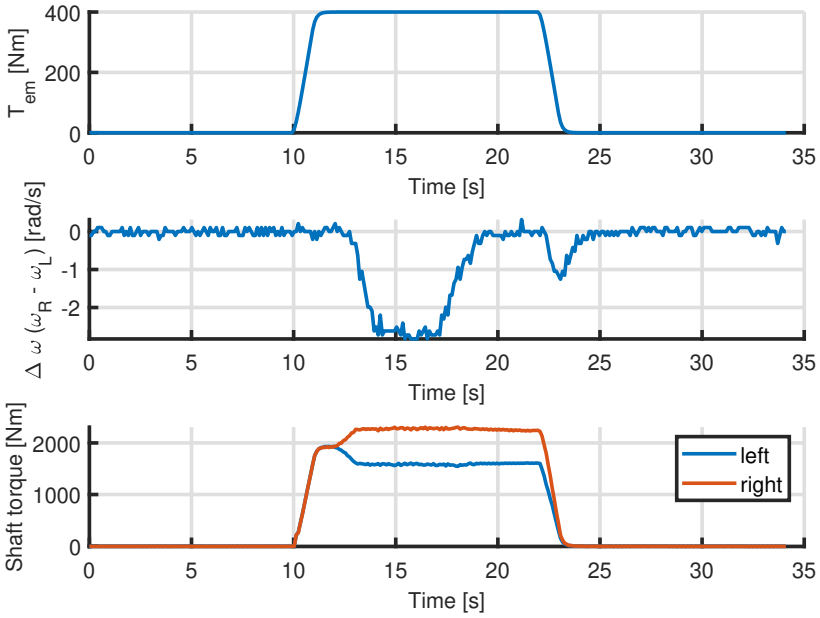

Figure 3.22: The dynamomoter data for various drive unit torques

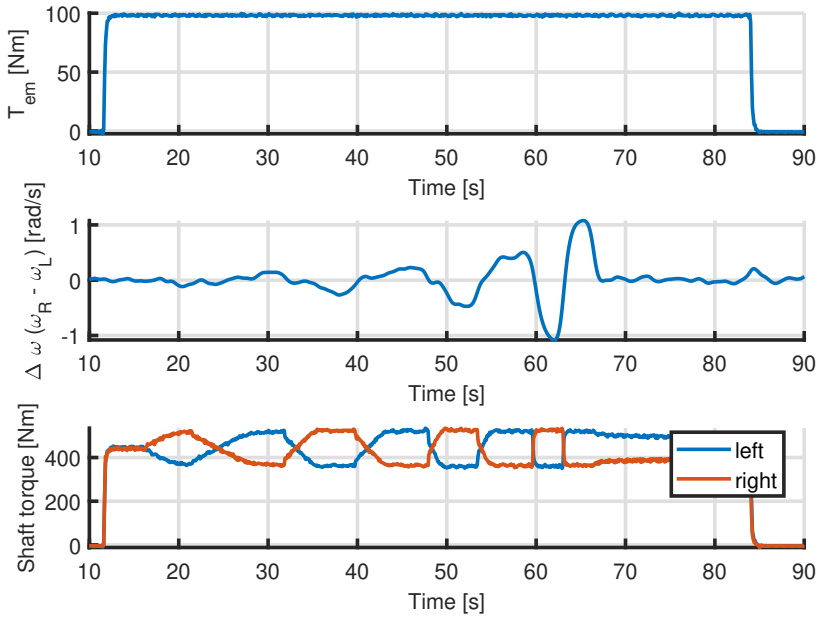

Figure 3.23: The dynamomoter data for various half shaft speed deltas

Creating a detailed physical model of the differential is not possible, as the true root cause of the internal friction is unknown. Researching this is outside the scope of this project and therefore an analytical representation of the observed behaviour will be created. The differential model computes the two torques which are applied to the left and right drive shafts. These two torques are given by

$$T_l = \frac{1}{2}T_{em} + T_{bias}$$
$$T_r = \frac{1}{2}T_{em} - T_{bias}, \tag{3.7}$$

where T_l and T_r are the left and right drive shafts torques respectively, T_{em} is the applied motor torque and T_{bias} is the computed torque bias. The torque bias is determined by integrating the torque bias rise rate and saturating the output. This is then multiplied by the maximum torque bias amplitude to find the torque bias. The relationship for the torque bias T_{bias} is given by

$$T_{bias} = G_{bias}|T_{em}| \int f_{t_r}(T_{em}, \Delta\omega), \tag{3.8}$$

where G_{bias} is a gain relating the motor torque to the maximum torque bias amplitude, f_{t_r} is the torque bias rise rate function and $\Delta\omega$ is the speed delta between both axles. The torque bias rise rate and magnitude were determined for various combination of motor torque and drive shaft speed deltas from the data from the dynamometer test. Table 3.4 presents the rise rate of the torque bias in various conditions, while Table 3.5 shows the steady-state torque bias magnitude measured. G_{bias} and $f_{t_r}(T_{em}, \Delta\omega)$ were determined by fitting curves to them. The limited sample size does reduce the accuracy. Additional testing has been requested, but these tests could not be completed in time.

Table 3.4: Torque bias rise rate [Nm/s]

		T_{em} [Nm]	
		100	200
$\Delta\omega$ [rpm]	1	33.3	-
	2	61.1	48.7
	4	118.9	106.7
	10	324.0	245.0

Table 3.5: Torque bias magnitude [Nm]

		T_{em} [Nm]	
		100	200
$\Delta\omega$ [rpm]	1	150.0	-
	2	165.0	302.0
	4	178.3	331.0
	10	162.0	343.0

To validate the differential the dynamometer is modelled in a separate environment. By using the motor torque, speed profile and shaft speed delta the resulting torque outputs can be compared to what has been measured. The results of the model under varying torques at a constant shaft speed delta are presented in Figure 3.24, while Figure 3.25 depicts the results of a simulation with a constant load, but varying shaft speed deltas. From these figures can be concluded that the differential torque bias matches the amplitude for the various motor loads exerted. The method for computing the torque bias is not perfect and may be refined more. However, the behaviour of the torque increasing over time is captured in the model. The response at small shaft speed deltas leaves something to be desired. At lower shaft speed delta the simulated torque bias lags behind the measured torque bias. The cause of this could also be the noise seen in the shaft speeds used as inputs as the signal-to-noise ratio is relatively low in the region of smaller shaft speed deltas.

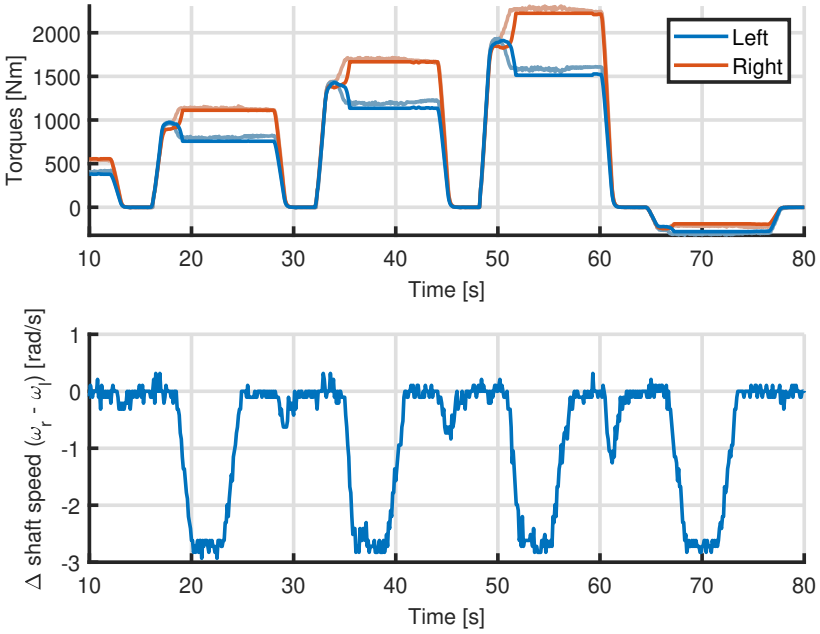

Figure 3.24: The validation of the differential model under varying load

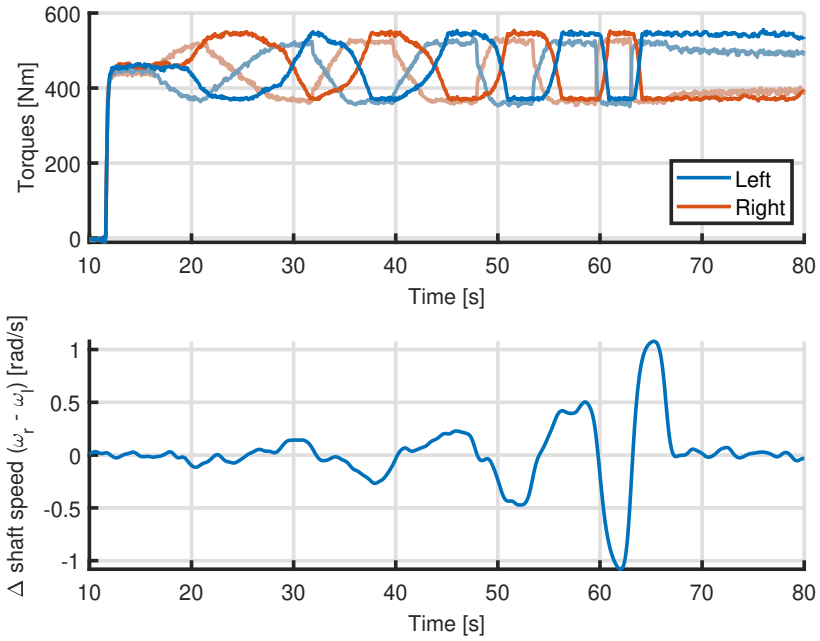

Figure 3.25: The validation of the differential model under varying shaft speed deltas

Having implemented the differential into the vehicle a validation run has been performed. The data presented in Figure 3.26 and Figure 3.27a shows that the torque bias is correctly simulated. However, when performing a wide open throttle where the steering wheel is kept perfectly straight, no torque bias is generated as presented in Figure 3.27b. This is due to the fact that the torque

bias is dependent on a wheel speed delta. When the vehicle is driving in a straight line a wheel speed delta is not observed. Interestingly, a delta in wheel speed is present in the measurement data, which explains the presence of a torque bias in the measurement data.

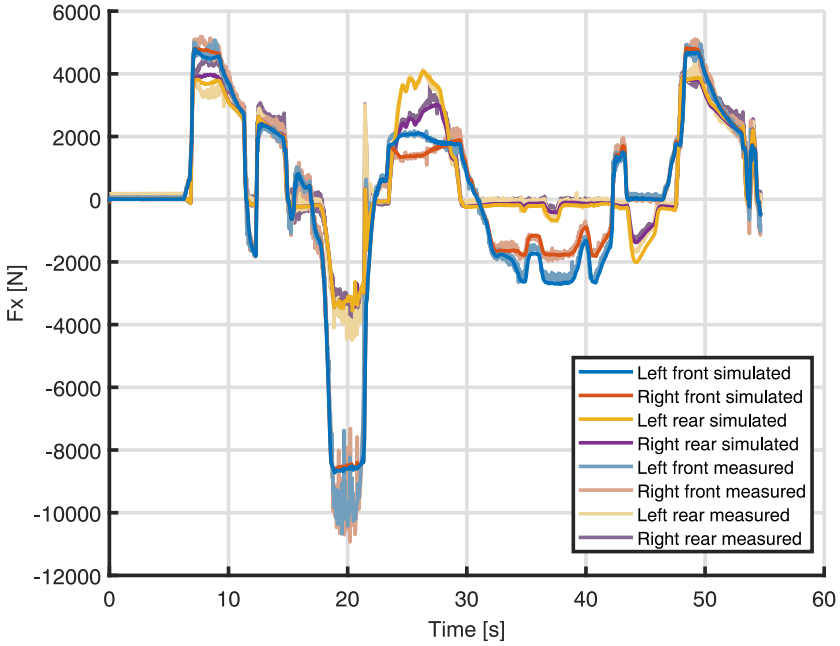

Figure 3.26: The validation of the differential model implemented into the vehicle

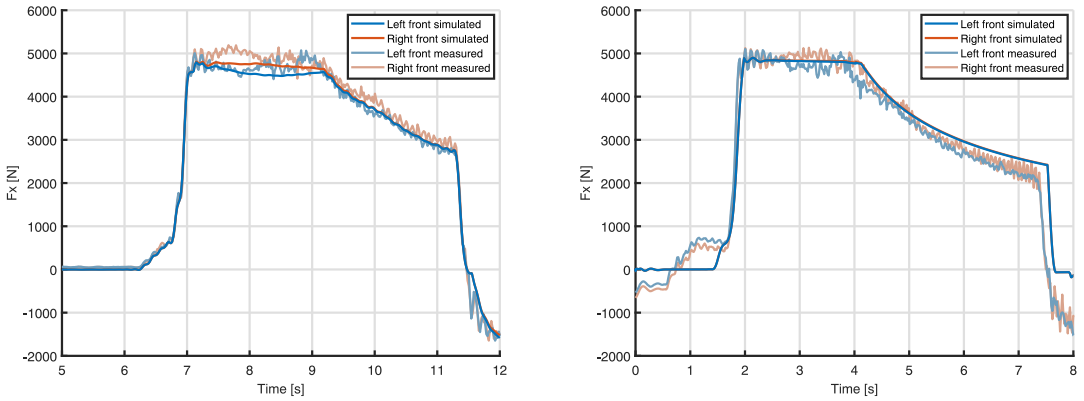

(a) Manoeuvre steering input

(b) Perfect straight line

Figure 3.27: The validation of the differential model implemented into the vehicle

The cause of the torque bias observed in a straight line is presumed to originate from the asymmetrical spring rates. Asymmetrical air spring pressures result in different spring forces. A plane which is height-adjusted on its four corners is over-constraint. Due to this one or two struts will always carry less load. In this instance, the front right-rear left diagonal has higher pressures and carries more load as confirmed by the measurement data. According to the relationship for κ, F_x and F_z the wheel slip necessary to achieve a certain tractive force reduces with an increase in F_z

[2]. Therefore, the wheel slip of the right tire should be smaller than the left tire. The wheel slip is calculated by

$$\kappa = \frac{v_x - \omega r_e}{v_x} \tag{3.9}$$

Therefore a difference in wheel slip provides a wheel speed delta as the effective tire radius and forward velocity, v_x, can be considered equal. This wheel speed difference will then cause the differential to bias the torque even when driving in a straight line. As the front left tire has a lower vertical force it slips more hence it will be rotating faster thus torque will be biased to the front right wheel.

Re-evaluating the same simulation now including the revised spring rates yields a torque bias both mid-corner as well as during straight-line acceleration as depicted in Figure 3.28b. Furthermore, it improves the behaviour for the simulation, which uses the inputs of the driver rather than steering rack displacement as inputs as highlighted in Figure 3.28a.

Half shafts are implemented to connect the differential to the wheel. These are modelled using the 'Simscape Constant Velocity' joints. These joints will produce an additional moment around the kingpin as seen in a real constant velocity joint. This is crucial to capture the effects of varying half-shaft angles.

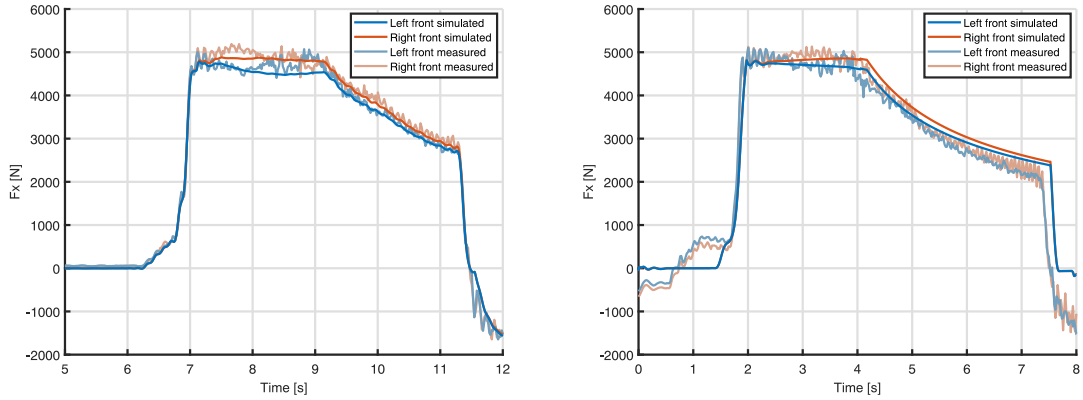

(a) Manoeuvre steering input

(b) Perfect straight line

Figure 3.28: The validation of the differential model implemented into the vehicle with asymmetrical spring rates

3.8 Full Vehicle Validation

A final validation can be performed now that all relevant subsystems are implemented. This is done by re-evaluating the same simulation. The complete set of figures generated by this simulation is included in Appendix A.2.

The inclusion of both the motor mount, steering rack and the differential into the chassis yields the expected results. The tie rod forces during a wide open throttle increases from 1.87 kN and 1.93 kN to 1.87 kN and 2.11 kN for the left and right tie rod respectively. Subsequently, this increases the force on the steering rack by 0.20 kN. This is also reflects in the steering wheel torque required to maintain the reference steering angle, which increases by an average of 0.5 Nm from the steering rack validation simulations done. Furthermore, even with the influences of other subsystems, the driver model can track the reference. It does oscillate a little more during and after a wide-open throttle. However, this is also something that is observed in the steering wheel angle produced by humans during such a manoeuvre.

As expected, the motor mount and differential do not impact each other. One aspect where they could influence each other is in the friction in the CV joints. As the angle of the drive shaft increases its friction will also increase. As the inclination angles do not alter equally the friction internal to the drive shaft differs as well. This will influence the torque bias in the differential. However, as the friction in the drive shafts is omitted this is not noticeable and the tractive forces produced are the same when only the differential is included.

The path of the vehicle is closer to the measured path with the inclusion of the three subsystems as depicted in Figure 3.29. This improvement is largely due to the torque bias produced by the differential. This introduces a counter-clockwise yaw moment which reduces the divergence to the right.

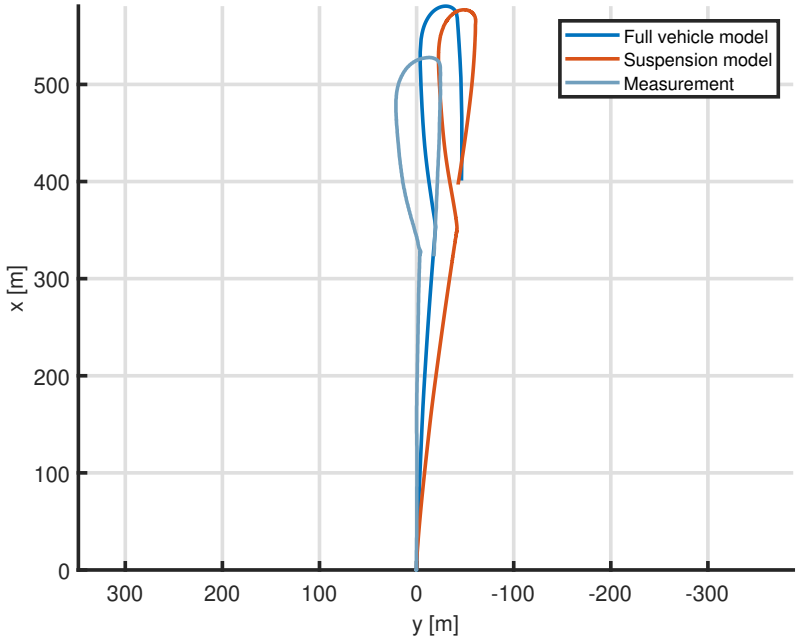

Figure 3.29: The trajectory during the validation of the complete model

4 Torque Steer Testing Results

Now that the vehicle and all its relevant subsystems are modelled and validated, it can be used to look into how much each component contributes to the torque steer behaviour. The behaviour will be analysed further to gain a better understanding of why it produces torque steer in the first place. This knowledge will aid exploring possible mitigation strategies for the torque steer behaviour present in the vehicle.

4.1 Quantification

To properly compare various configuration a quantification system needs to be set up as torque steer is not defined by a single specific force. In this research the amount of torque steer will be quantified based on four signals:

- *Steering rack force*: The force applied to the steering rack when holding the steering wheel at zero degrees.
- *Torsion bar torque*: The torsion bar torque required to keep the steering wheel at zero degrees.
- *Lateral position deviation*: The lateral deviation from a straight line after 140 m when not holding the steering wheel
- *Steering wheel angle*: The maximum change in steering wheel angle when not holding the steering wheel.

4.2 Simulations

Simulations of various vehicle configurations can be performed With the model completed. This section will present the results of the simulations done to find the individual component contributions as well as the effectiveness of possible mitigation strategies.

4.2.1 Torque Steer Contributors

The first set of simulations revolves around obtaining the contribution of the various subsystems to the torque steer problem. For this quantification, maximum acceleration runs will be performed for various combinations. The simulation will be repeated both with hands on and hands off the steering wheel to capture the vehicle path, steering rack force, steering wheel angle and steering wheel torque. The front drive unit torque profile from the measurement data, depicted in Figure 4.1, is used for these simulations.

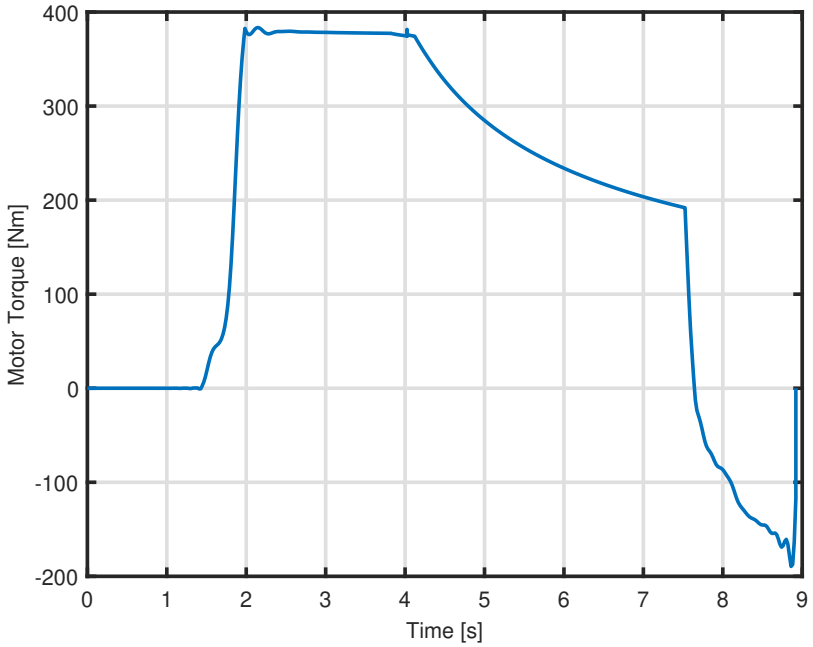

Figure 4.1: The motor torque profile used for the simulations

In total six different configurations are evaluated as presented in Table 4.1. First, a baseline simulation is performed excluding the motor mount, differential and asymmetrical spring rates. Next are simulations including various combinations of the three aforementioned subsystems. These are being executed twice, once without hands on the steering wheel and once with, keeping the steering wheel at zero degrees.

Table 4.1: The various components included in the vehicle simulation

	Deflecting motor mount	Torque biasing differential	Asymmetrical spring rates
Simulation 1			
Simulation 2	X		
Simulation 3		X	
Simulation 4			X
Simulation 5		X	X
Simulation 6	X	X	X

The results of these simulation are presented in Figure 4.2. The results show that the base vehicle does not deviate from a straight line. This is due to it not generating steering rack forces as it is completely symmetrical. Initially is was suspected that the suspension geometry itself might contribute to torque steer as its wheel centre offset change unfavourably. The suspected steering instability does, however, not show when accelerating. The self-aligning characteristics of the suspension and the tires overcome this effect suppressing it and stabilising the steering system.

Once the motor mount is introduced the vehicle starts to show torque steer. This is due to it deflecting and raising one drive shaft output higher than the other. This deviation in drive shaft angle results in varying kingpin moments. The result is a steering rack force which is directly proportional to the torque applied by the motor. Furthermore, the steering wheel will be rotated to a maximum of 4.6°. Consequently the vehicle will deviate from a straight line. It will veer to the left as much as 8.4 m after having driven 140 m. To correct this a driver would have to apply a peak

torque of 0.24 Nm to the steering wheel.

Running the simulation only including the differential will not result in torque steer, as the differential will only start to bias torque if there is a wheel speed difference present. With the vehicle driving in a straight line this does not occur hence no torque steer is observed in this case. This is reflected in the trajectory which is as straight as the baseline simulation and in the rack force and steering wheel torque which remain zero.

The same goes for the asymmetric spring rate by itself. Although it will deviate a little more from a straight line compared to the baseline and differential, it does not generate steering rack forces and barely rotates the steering wheel.

Torque steer will once again be noticeable once the differential and the asymmetric spring rate are combined. The way the torque steer exhibits itself is very different from the torque steer caused by the motor mount. Due to the ramp-in effect the steering rack force slowly increases until it reaches a maximum. As a result the steering wheel angle varies less than the motor mount. However, the path is matching the one of the motor mount. This is due to the torque bias causing an additional yaw rate besides the vehicle steering.

The vehicle will deviate significantly more from a straight line When all subsystems are included. Within 140 m the vehicle will have moved 15 m to the left. The steering rack force is a summation of the motor mount simulation and the differentials with asymmetric spring rate simulation. The peak force is therefore about double the peak of the maximum seen in the individual simulations. The same doubling can be observed in the other metrics.

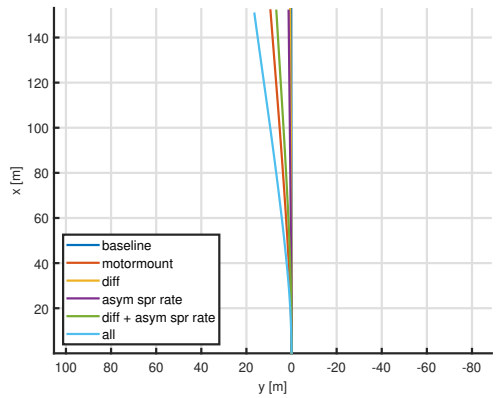

(a) The trajectories of various hands off wide open throttle simulations

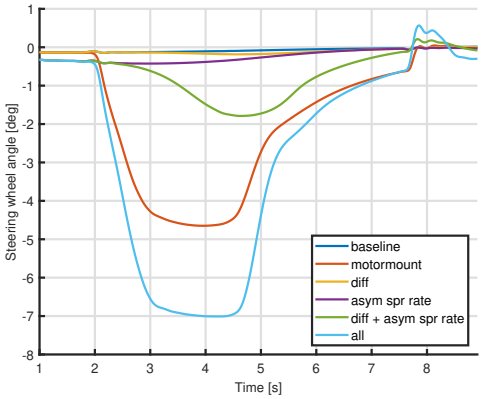

(b) The steering wheel angles of various hands off wide open throttle simulations

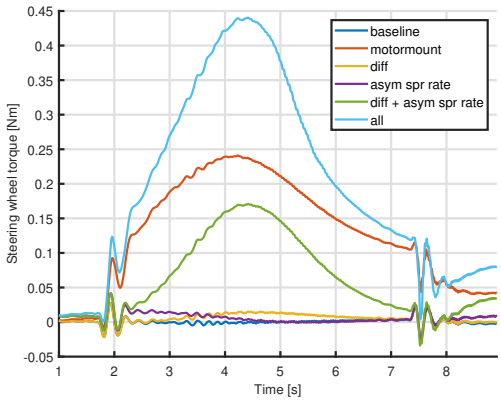

(c) The steering wheel torque of various hands on wide open throttle simulations

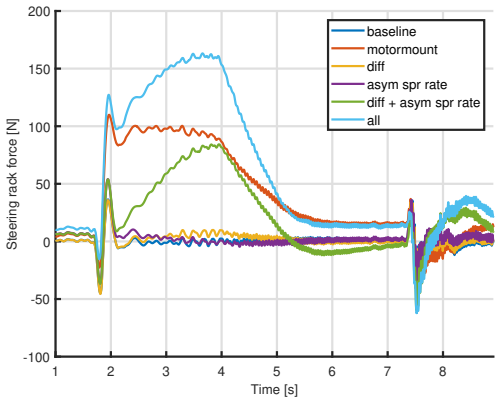

(d) The steering rack force of various hands on wide open throttle simulations

Figure 4.2: The torque steer quantification for various vehicle subsystem configurations

4.2.2 Torque Steer Mitigation Strategies

Torque steer mitigation strategies can be investigated now that the root cause is known. The obvious solution would be to redesign the motor mount and resolve the air spring and differential issues. This would eliminate torque steer, but it would only be applicable to the next generation and not to the vehicles currently in production.

Model 3 Motor Mount

Something that has already been explored is a redesigned motor mount. As an experiment the rubber bushings were replaced with solid aluminium mounts. This prevented the motor from rotating and thus prevented torque steer due to varying half shaft inclination angles. The downside of this solution is the NVH issues it introduces. As the motor is solidly coupled to the chassis the vibrations generated by it are much more audible in the cabin and hence not suitable for a production vehicle.

A better solution would be to implement a motor mount which has a horizontal torque roll axis. The Model 3 already has such a mounting strategy, where there are two rear mounts at the same height and one in the front to control the roll, as depicted in Figure 4.3. With both half shaft angles remaining equal throughout an acceleration no torque steer will be generated.

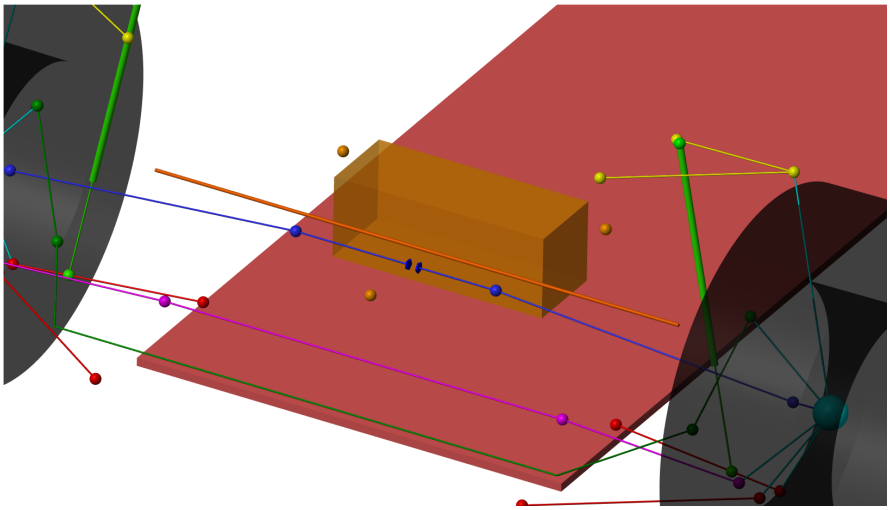

Figure 4.3: The Model 3 motor mounts

In the simulations the Model 3 motor mount has been included, while the differential and air suspension asymmetry have been excluded. Figure 4.4 shows that the vehicle only deviates 0.16 m after having driven 140 m. This is negligible compared to the original motor mount where the vehicle deviated 8.4 m after having driven the same distance. Furthermore, the steering wheel barely rotated when when accelerating only reaching a maximum angle of 0.1° compared to the 4.6° observed with the original mounting. The elimination of torque steer is also visible in the steering wheel torque required to keep the wheel straight, which is reduced from 0.239 Nm to nearly zero Nm. The complete set of results is included in Appendix A.3.

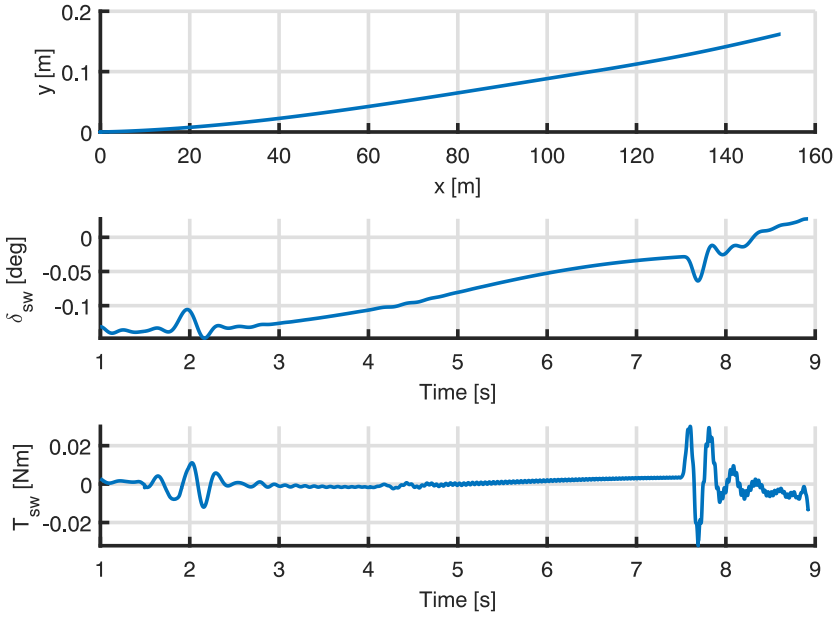

Figure 4.4: The simulation results of the vehicle with a Model 3 motor mount

Adjusted Air Suspension

As previously presented the asymmetric spring rate will cause a wheel speed delta under high acceleration even when driving straight. In many cases, the left rear air spring has a higher pressure. Therefore, a majority of the weight of the vehicle will be put on the front right and left rear tires. This results in a wheel speed delta where the front left tire rotates faster and thus torque is biased to the right. The consequence is that the vehicle will steer to the left. This also means that the vehicle will steer to the right when the left rear strut has a lower pressure and more load is put in the front left and rear right wheels. The simulation results show that with this change the right wheel rotates faster than the left wheel as depicted in Figure 4.5. Consequently, the torque is also biased to the left wheel hence its tractive force is larger.

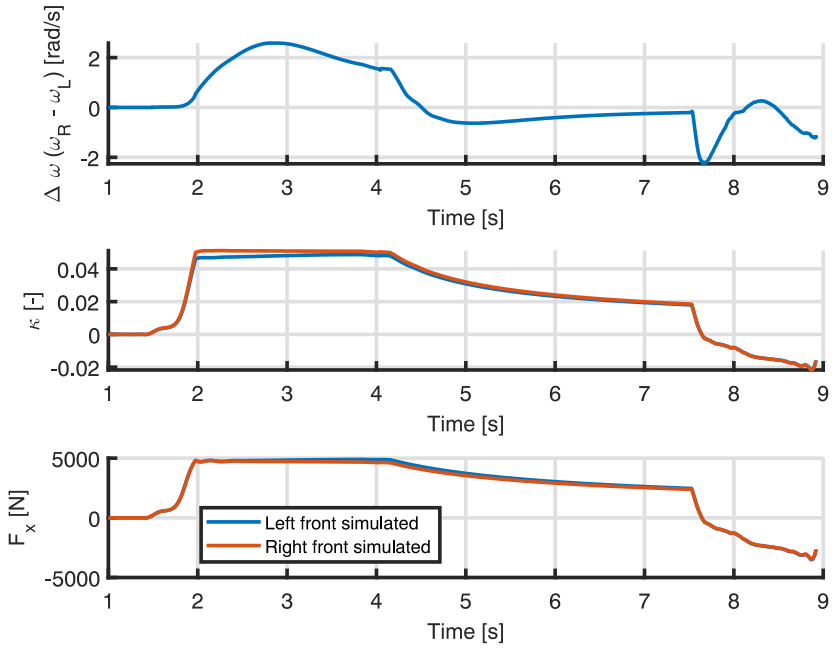

Figure 4.5: The tire data of the simulation of the vehicle with adjusted air suspension

Some steering wheel movement is, however, noticeable as it rotates to a maximum of 0.9° to the left as presented in Figure 4.6. This is due to the contribution of the differential and the motor mount varying slightly in magnitude. Due to this the path of the vehicle deviates slightly to the right while the steering wheel turns to the left. This is further enhanced by the now clockwise yaw moment generated by the differing tractive forces. The torque required to keep the steering wheel straight has reduce from a peak value of 0.45 Nm to 0.1 Nm.

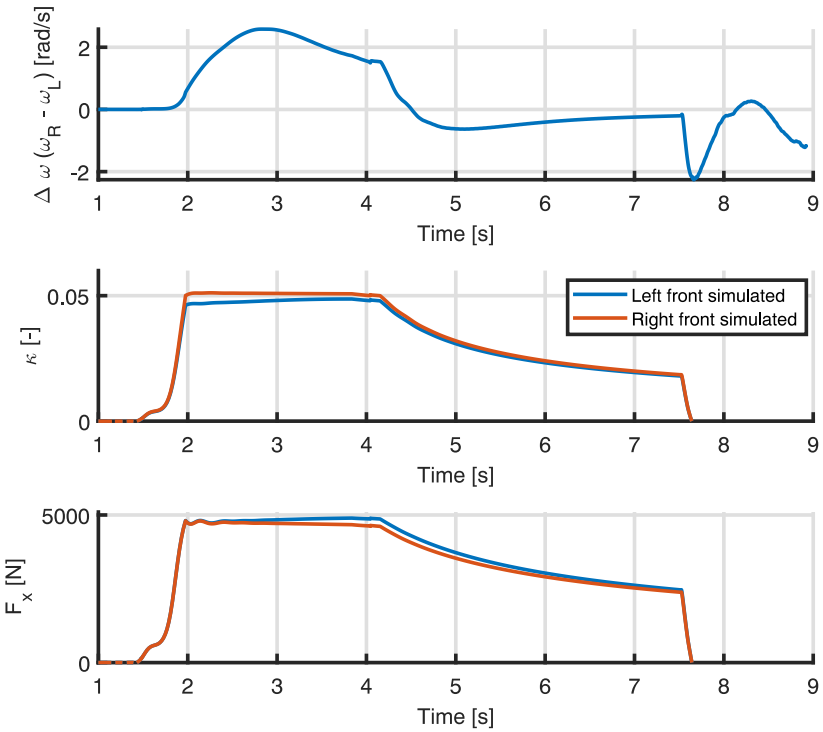

Figure 4.6: The results of the full vehicle with adjusted air suspension

The air suspension in the vehicle is controlled by software. Therefore, it should be possible to implement an algorithm which alters the pressures to swap the diagonal with the higher spring pressures. Torque steer can be then alleviated on the entire fleet without any significant costs. The alteration should also not influence the vehicle dynamics significantly, as currently there already is an asymmetry in the air suspension which has gone unnoticed. Mirroring the spring pressures should therefore not have a significant influence on the vehicle dynamics. The complete set of results is included in Appendix A.4.

4.3 Experiments

The model predicts that manipulating the air suspension pressure distribution will cause the vehicle to drive straight when performing a wide open throttle acceleration, without hands on the steering wheel. To verify this a test is performed on an real vehicle.

The vehicle will be levelled to get default spring pressures. A few hands-off wide open throttle accelerations will be performed to obtain a base line for the torque steer behaviour. During the acceleration the throttle pedal position, motor torque, steering wheel angle and wheel speeds will be measured. The air spring pressure will be lowered to about 10% less than the rear right air spring by manually manipulating the valves. The resulting air spring pressures are presented in Table 4.2. The same test is executed using the new air spring pressures.

Table 4.2: Air suspension pressures used during testing

Vehicle	Air suspension system	Pressures [Bar]	
2018 Refresh Model S	Tesla air suspension default	8.3	8.8
		6.0	5.4
2018 Refresh Model S	adaptive Tesla air suspension modified	8.7	8.5
		5.6	5.7

During the baseline test the steering wheel will start to rotate to the left as soon as any torque is applied as shown in Figure 4.7. At 6 seconds the vehicle path was corrected hence the sudden change in steering wheel angle to the right.

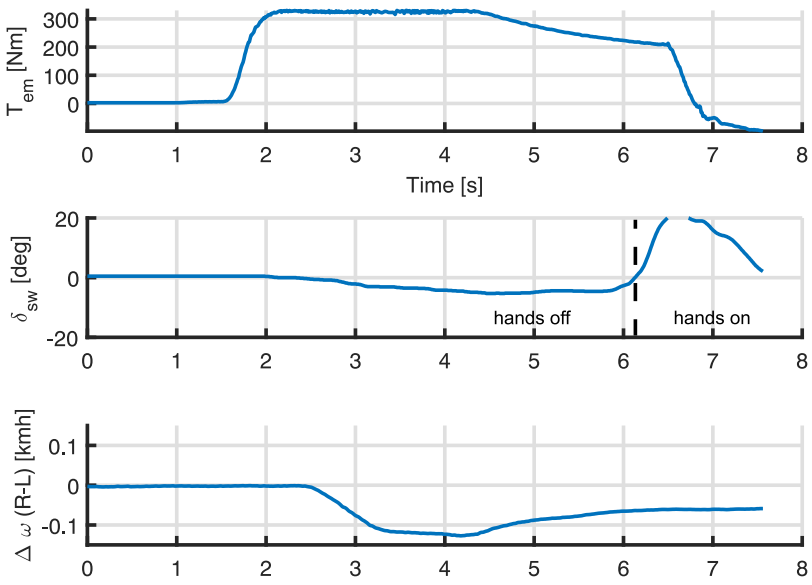

Figure 4.7: The baseline results of wide open throttle runs

Rerunning the same test with the modified air suspension yields the results depicted in Figure 4.8. Here intervention took place at 3.5s. The steering wheel rotates barely as soon as torque is applied, as the simulations predicted. As expected the wheel speed delta sign has changed. Now the left wheel is slower than the right wheel and therefore the torque is biased to the left wheel. The magnitude in wheel speed delta is much larger now. This could be due to the vehicle following a straight line where as it previously turned to the left which naturally causes the right wheel to rotate faster. Therefore, $\omega_R - \omega_L$ has a lower amplitude. 39

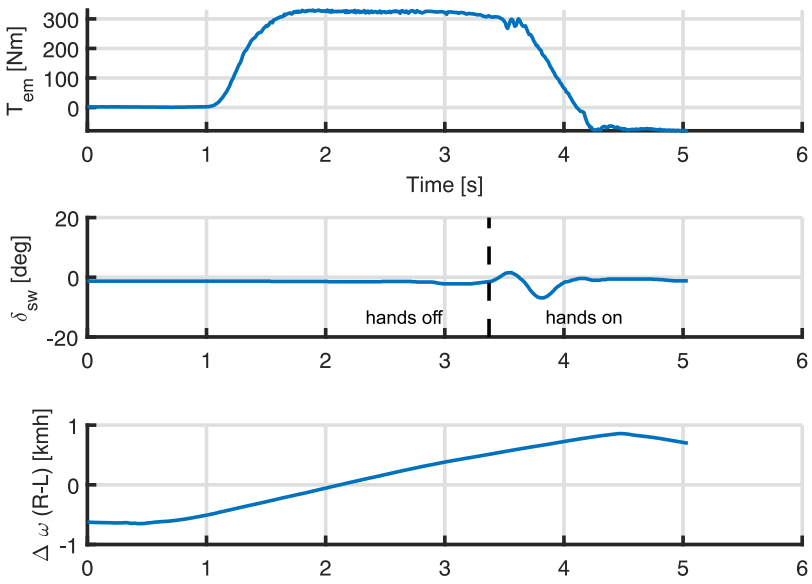

Figure 4.8: The results of wide open throttle runs with modified air suspension

The results of this experiment serve as a proof of concept for a possible mitigation of torque steer. Furthermore, the measured results reflect the predictions made using the simulations, which further strengthens the validity of the model.

5 Conclusions & Recommendations

5.1 Conclusions

This research aims to develop a multibody vehicle simulation model, find out what the root cause of torque steer is on an all-wheel drive Tesla Model S and how it can be reduced or eliminated. These questions have been answered through a literature study, the development of a simulation tool to analyse torque steer effects and experiments.

The root cause of the torque steer observed in the Tesla Model S is found to be due to a combination of three components; the motor mounts, the differential and the air suspension system. The motor mounts will deflect when the drive unit produces torque. The drive unit rolls around a non-horizontal axis due to the motor mount positioning. The consequence of this is that the half-shaft angles will deviate from one another under acceleration resulting in a force on the steering rack.

Dynamometer and vehicle validation tests show that the differential will bias torque to the slower wheel, similar to how a limited slip differential would. This indicates that there is some internal friction in the differential. The root cause of this bias is not fully understood and should be investigated further, but the hypothesis is that the high load deforms the cross pin about which the planetary gears rotate causing them to bind.

For the differential to start biasing torque a wheel speed difference should be present which should not be the case during straight-line acceleration. Tests have proven that this is the case. This is caused by the air suspension which has, in many cases, a higher rear left spring pressure. The consequence is that there are different loads on the front tires. They will produce different longitudinal wheel slips for a specific torque applied. This wheel slip will cause a difference in angular velocity as the longitudinal velocity of both wheels is the same. Therefore, the effects of the differential will only become apparent as soon as air suspension is considered as well.

A few approaches can be considered to mitigate torque steer. A reduction in allowed wheel slip in the traction control system would reduce the wheel speed difference. However, it will also limit the maximum torque output and thus hamper the performance of the vehicle, which is undesirable.

A redesign of the motor mount and differential would be the best solution. By implementing a mounting system with a horizontal torque roll axis, no difference in half-shaft inclination angle is observed anymore during acceleration. Furthermore, if the internal friction in the differential can be removed it would no long bias torque. The combination of these two changes will eliminate torque steer. This approach applies, however, only to a new vehicle design and not to the vehicles currently on the road.

The last approach is a rework of the air suspension firmware. The load asymmetry between the front tires can be swapped by lowering the pressure of the rear left air spring. In doing so the right front wheel will have less traction, will slip more, will start to rotate faster and therefore the differential will bias torque to the left front wheel. This will counteract the torque steer produced by the motor mount. This has been tested on an actual vehicle and the results show that it is indeed possible to mask torque steer from the driver by manipulating the air suspension system.

5.2 Recommendations

Although the root cause of the torque steer has been found and a mitigation strategy has been proposed, there are still some questions that are left unanswered. This chapter discusses those tasks which were outside of the scope of this project either due to time or complexity constraints.

Torque Steer Analysis Tool

The tool is capable of simulating the torque steer of a vehicle including or excluding various subsystems. However, a few features are missing or could be improved.

Firstly, the scope of the project is limited to rigid bodies. This is, however, not the case in actual vehicles. The model could be improved by including the deformation of parts besides the bushings in the front suspension. Most notably the drive shaft should include torsional deformation. As highlighted previously the left and right drive shafts are often not the same for packaging reasons. Therefore, their torsional stiffness could differ. The Simscape library allows easy implementation of flexible bodies, however the model is currently not able to simulate this without taking an unacceptable amount of time due to computational constraints.

Furthermore, while researching it became apparent that the springs are more relevant than initially thought. Therefore, it would be beneficial to add the option to replace the coil springs with a more detailed air spring model. This would allow simulations using the measured air spring pressures instead of an approximation model to reflect the change in spring rate due to differences in air spring pressure.

Differential

It has been shown that the differential is not truly an open differential and that it will bias torque. The root cause of this has not yet been investigated.

It is beleived that there is internal friction in the differential which causes this. The ramp-in effect indicates that there is some increase in friction as the planetary gears start to rotate. The locking effect can only be sustained if a friction force is present in absence of a wheel speed difference.

The source of this friction could be the friction between the planetary gear and the cross-pin. There will be a large normal force on the bevel gears and the cross-pin due to the high torque applied to the differential. Even with a small coefficient of friction, the friction force could already be significant. Moreover, due to the high forces, the lubrication might fail, increasing the coefficient of friction.

Another possible cause could be the deformation of the pin around which the planetary gears rotates. Reference [8] has shown that in this type of differential there is little deformation in the outer housing, however, the pin deforms more easily.

Researching this further would prove to be beneficial as it could improve future differential designs. The current proposed solution exploits the undesirable characteristics of the differential to cancel out the undesirable characteristics of the motor mount. Researching the root cause of the torque bias would, however, be a graduation project by itself .

Air Suspension

The air suspension was found to have asymmetrical air spring pressures across the four corners of the vehicle. This provoked the differential to bias torque even when driving in a straight line. The reason for this asymmetry has not been investigated extensively.

It was noted that the rear left air spring often has a higher pressure after levelling. However, if the vehicle would sit overnight this deviation grows. This could be caused by a firmware issue or a hardware problem, such as a leak somewhere. As this behaviour has been noted across multiple vehicles and multiple models the latter is however less likely.

During levelling the air suspension controller will level each axle to a target height and the pressures are not taken into consideration. To achieve a higher pressure there would have to be more load on the rear left strut. It could also be possible that the vehicle body is slightly twisted due to the stacking of manufacturing tolerances.

The pressure difference does allow the differential to bias torque when driving in a straight line. Therefore, it may be beneficial to dive deeper into this topic. There would have to be some changes made to the air suspension firmware as well if the proposed mitigation were to be implemented.

References

[1] J. Dornhege and Ford Werke, "Torque steer influences on McPherson front axles."

[2] I. Besselink, *Vehicle Dynamics – 4AT000 Lecture notes*. 2020.

[3] J. Balkwill, *Performance Vehicle Dynamics: Engineering and Applications*. Butterworth-Heinemann, ISBN: 978-0128126936.

[4] "On the torque steer problem for front-wheel-drive electric cars," Springer, 2020, pp. 1103–1124, ISBN: 9783030410568. DOI: 10.1007/978-3-030-41057-5_90.

[5] "On the influence of suspension geometry on steering feedback," *Applied Sciences (Switzerland)*, vol. 10, 12 Jun. 2020, ISSN: 20763417. DOI: 10.3390/app10124297.

[6] S. Woo, S. Park, and Y. Oh, "Solution for the torque steer problem of a front-wheel drive car with a high-torque engine in vehicle development stages," *SAE Technical Paper 2007-01-3656*, 2007.

[7] M. Gadola, D. Chindamo, and B. Lenzo, "Revisiting the mechanical limited-slip differential for high-performance and race car applications," *Engineering Letters*, vol. 29, 3 2021, ISSN: 18160948.

[8] M. O. Bernades, "Torque split between left and right drive shaft over a front wheel drive differential," *Chalmers University of Technology*, 2012, ISSN: 1652-8557.

[9] D. W. Mikels and Y.-J. Seo, "Independently suspended and driven asymmetric axle shafts," US 7,938,222 B2, 2011.

[10] M. Frantzen, W. David, M. Simon, and L. Ohra-aho, "Less torque steer effect," 2004.

[11] M. Frantzen, J. Bouma, W. David, M. Simon, and L. Ohra-aho, "The simple answer to torque steer: 'revo' suspension," 2004.

[12] J. Dornhege, "Torque steer compensation using epas," *13th European Automotive Congress*, 2011.

[13] J. Dornhege, S. Nolden, and M. Mayer, "Steering torque disturbance rejection," *SAE International Journal of Vehicle Dynamics, Stability, and NVH*, vol. 1, pp. 165–172, 2 Mar. 2017, ISSN: 23802162. DOI: 10.4271/2017-01-1482.

[14] G. Hisar and O. M. Navarro, "Torque steer mitigation using electric power steering (eps) system," *Diploma work - Department of Applied Mechanics, Chalmers University of Technology, Göteborg, Sweden*, 2007.

[15] B. Rensen and I. J. M. Besselink, "Design and analysis of a multi-link suspension for a 4wd formula student racing car," 2019.

A Appendix

A.1 Torque Steer Simulation Tool Instructions

The tool is developed in Matlab/Simulink. The software packages used and their respective versions are listed in Table A.1.

Table A.1: The simulation tool dependencies

Package	Version
Matlab	2022a
Simulink	10.5
Simscape	5.3
Simscape Multibody	7.5
Curve Fitting Toolbox	3.7
Signal Processing Toolbox	9.0

Running a simulation

The tool itself is split into 6 parts:

- *Input handlers*: Generates or loads input and measurement signals to be used during the simulation or analysis afterwards.
- *Vehicle handlers*: Generates or loads the parameters for a specific vehicle to be used during simulation
- *Tire handlers*: Load the Magic Formula tire parameters from a `.tir` file to be used during simulations
- *Simulink files*: Contains all the Simulink `.slx` files to simulate each subsystem or the entire vehicle
- *Simulation handlers*: Contains all pre- and post-processing functions needed when running a simulation, including the plotting of the results
- *Library*: Contains miscellaneous functions available to be used by all files mentioned about

To run a simulation the `multibody_model.m` file needs to be executed. This will trigger the input generation, loading of the vehicle and tire parameters, perform any pre-processing, execute the Simulink, post-process the data and visualise it. A selection of which figures to generate can be made in the `multibody_model.m` file. A selection of which simulation to perform can be selected here by altering `sim_type`. The options are:

1. Suspension Kinematics: Vertical height dynamics and steering sweep dynamics
2. Suspension Kinematics: measurement data input
3. Full vehicle: No inputs
4. Full vehicle: Steering wheel step response
5. Full vehicle: Measurement data based wide open throttle
6. Full vehicle: Custom input wide open throttle
7. Full vehicle: Measurement data based wide open throttle, 1G braking, cornering

8. Full vehicle: Automation of validation for multiple configurations
9. Steering Rack: Measurement data based wide open throttle, 1G braking, cornering
10. Motor Mount: Torque sweep
11. Differential: Dynamometer test

The automation of validation runs a simulation multiple times configuring the vehicle differently every execution. This can be set up in the `multibody_model` file. In the `runs` variable the settings for every run can be defined. In this variable, each cell represents a simulation and every line in such a cell is a piece of Matlab code that will be executed before the simulation is started. The results of every simulation will be stored automatically in a folder. Afterwards, the `analysis` can be used to create the figures to compare the results of the various simulations executed.

The various configurations of the vehicle can be created in the `multibody_model.m` file by setting the desired values. The options are:

1. Human driver: Use the human driver model (1 or true) or use the direct steering rack displacement (0 or false).
2. Hands-on: The human driver should hold the steering wheel (1 or true) or should keep its hands off (0 or false). No effect when the human driver is disabled.
3. Fixed motor mount: The motor mount should be rigid (1 or true) or should allow deflection (0 or false).
4. Fixed motor mount angle: The fixed motor mount angle or rotation around the torque roll axis in degrees. No effect when the motor mount is not fixed.
5. Torque bias: Enable (1 or true) or disable (0 or false) the differential torque bias.
6. RL shock pressure gain: A gain to alter the rear left air spring pressure.
7. M3 motor mount: Use the original motor mount (0 or false) or the Model 3 motor mount (1 or true).

Adding a simulation

Start by adding a new case with a unique integer to the `multibody_model` to add a new simulation to the tool. In this new case any pre-processing or setup can be entered before running the simulation. Then the desired Simulink file can be run. and any post-processing can be done afterwards. Then add case with the same integer to the `input_generation` script. In this case the vehicle, tire and the inputs to the simulation have to be defined. Additionally, the loading of the measurement data can be done here as well. Lastly, an if statement comparing `sim_type` to the new case integer has to be added to the `figures` script. In this if statement block the creation of the figures can be defined.

Adding a vehicle

Create a new vehicle parameter function in the vehicle handler folder to add a vehicle to the tool. This function should return a single data structure containing all the required parameters. To make the new vehicle available it has to be added to the `get_vehicle` function. Add a new case to this function with a unique key, call the newly added vehicle parameter function and assign the return data to the vehicle variable. The vehicle can now be selected in the input handler by calling `get_vehicle` with the key as input.

Adding a tire

Adding a new tire works similarly to adding a new vehicle. Move the `.tir` file describing the Magic Tire Formula parameters to the tire handler folder. Add a new case with a unique name to the `get_tire` function and set the filename which should be used for the front and rear tire respectively. The function will then load the parameters from the file to be used in the simulation. The tire can now be selected in the input handler by calling `get_tire` with the key as input.

A.2 Full vehicle model hands off wide open throttle simulation results

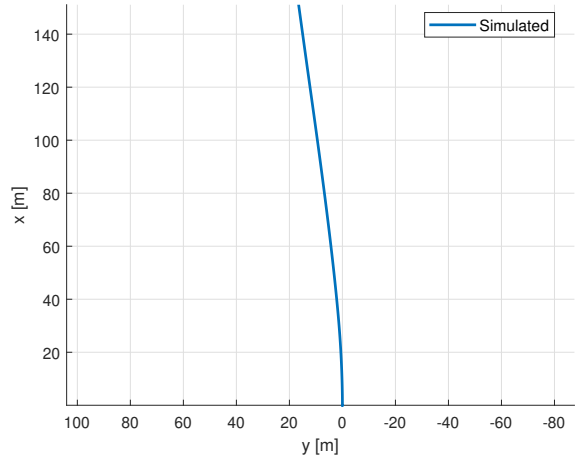

(a) The vehicle path

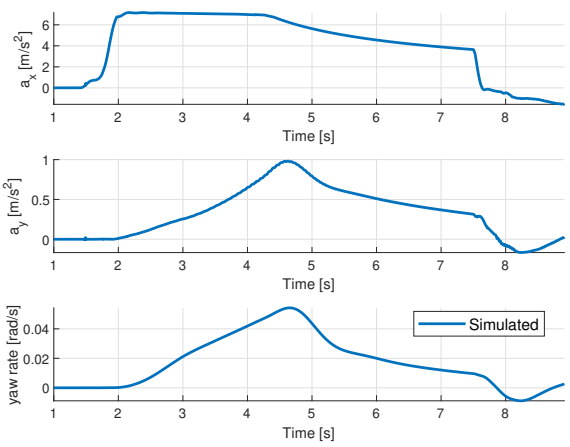

(b) Vehicle accelerations

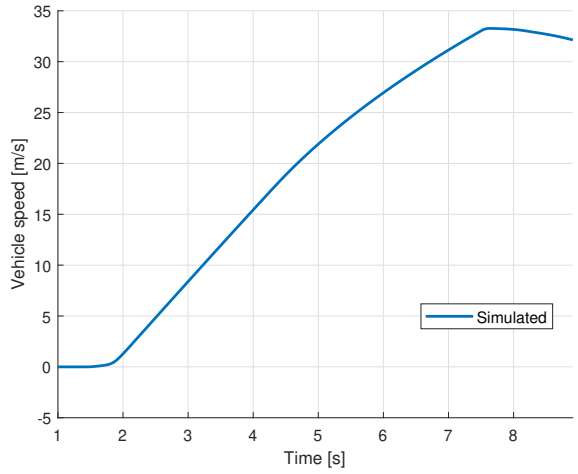

(c) Vehicle velocity

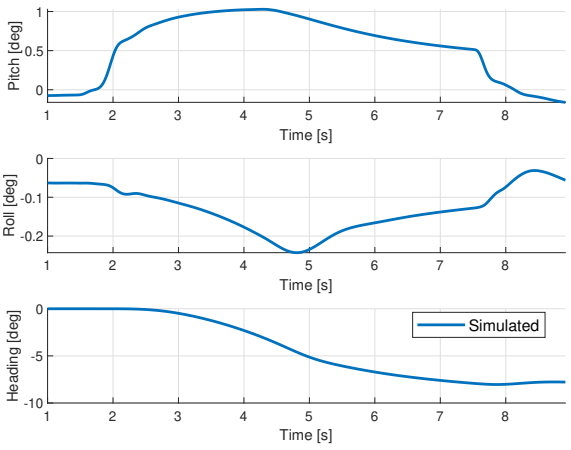

(d) Vehicle roll, pitch and heading angles

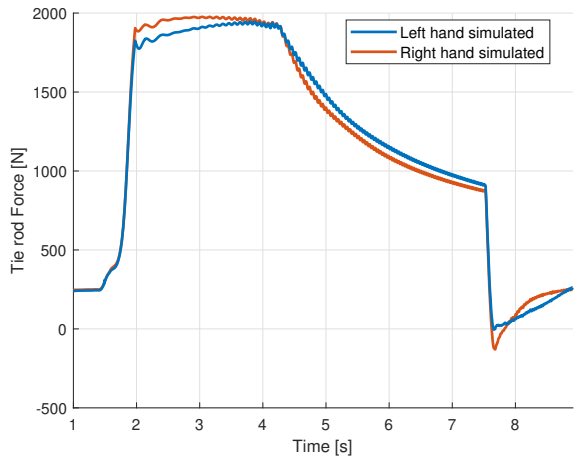

(e) Tie rod forces

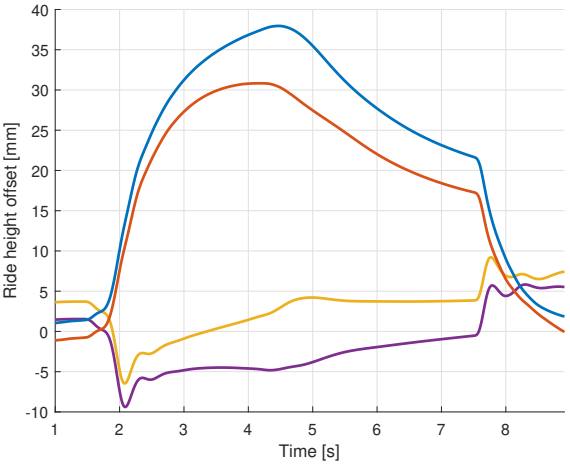

(f) Ride height

Figure A.1: The vehicle simulation results

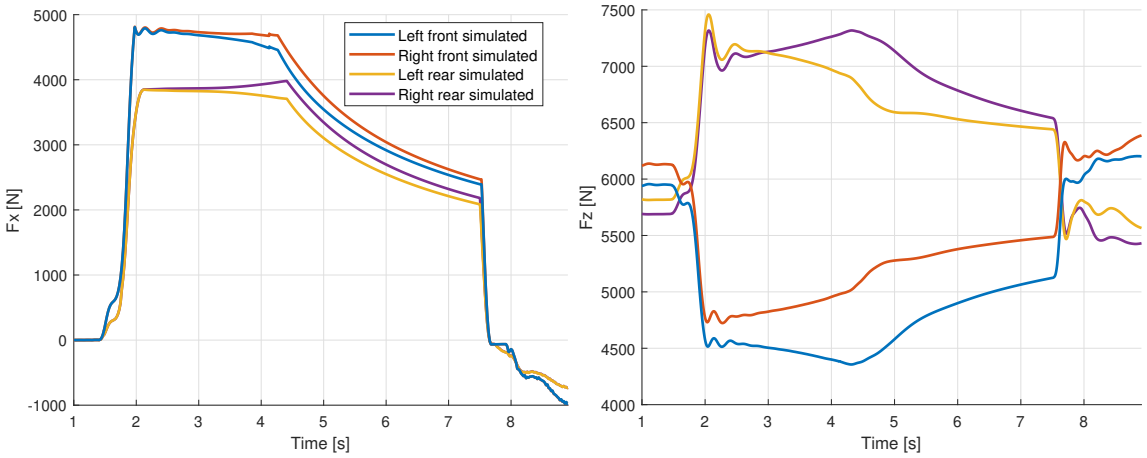

(a) Tractive force (F_x)

(b) Vertical force (F_z)

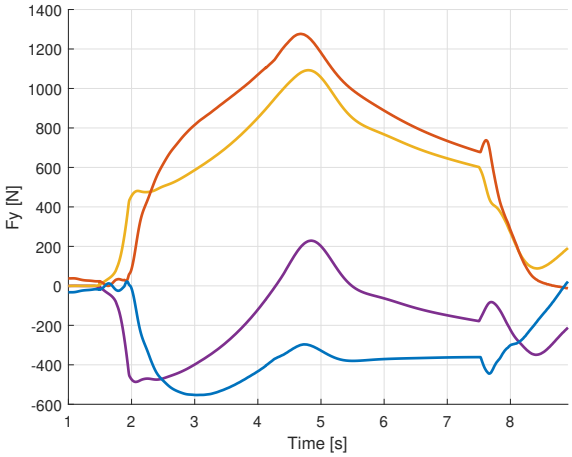

(c) Lateral force (F_y)

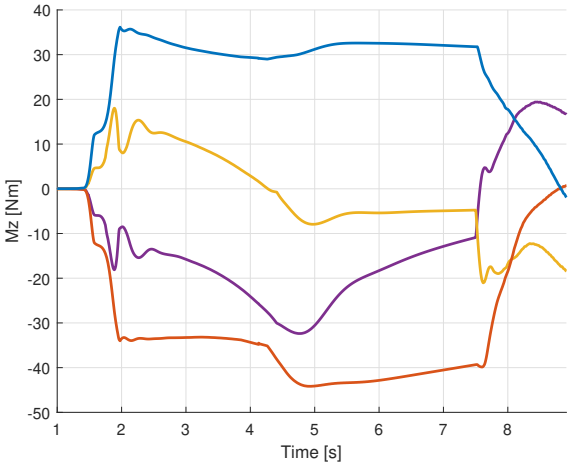

(d) Self aligning moment (M_z)

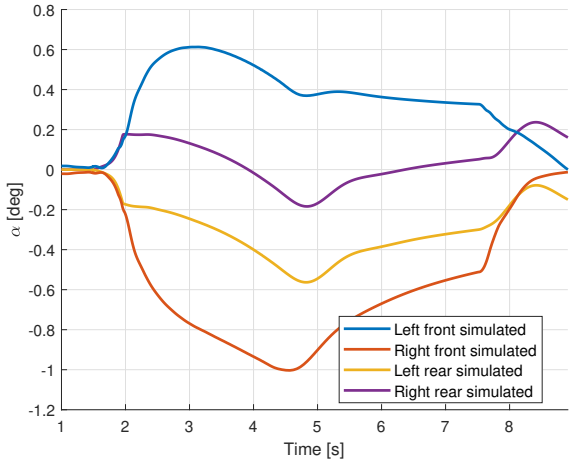

(e) Slip angle (α)

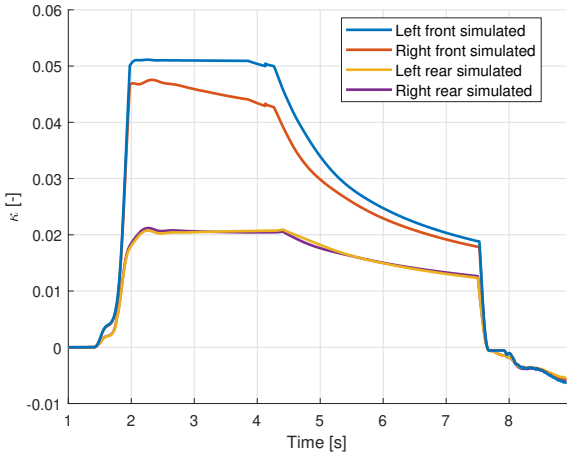

(f) Longitudinal slip (κ)

Figure A.2: The Tire simulation results

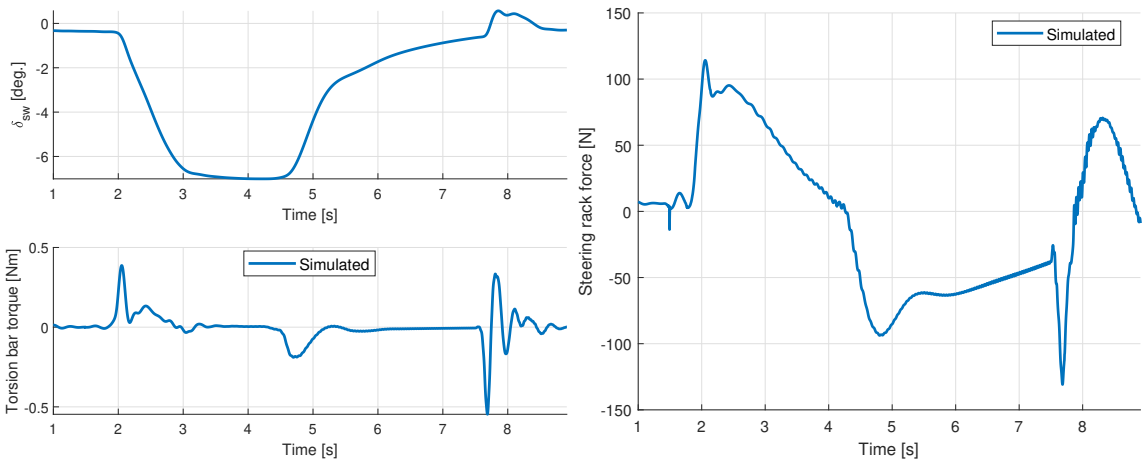

(a) Steering wheel position and torque

(b) Steering rack force

Figure A.3: The steering system simulation results

A.3 Model 3 motor mount hands off wide open throttle simulation results

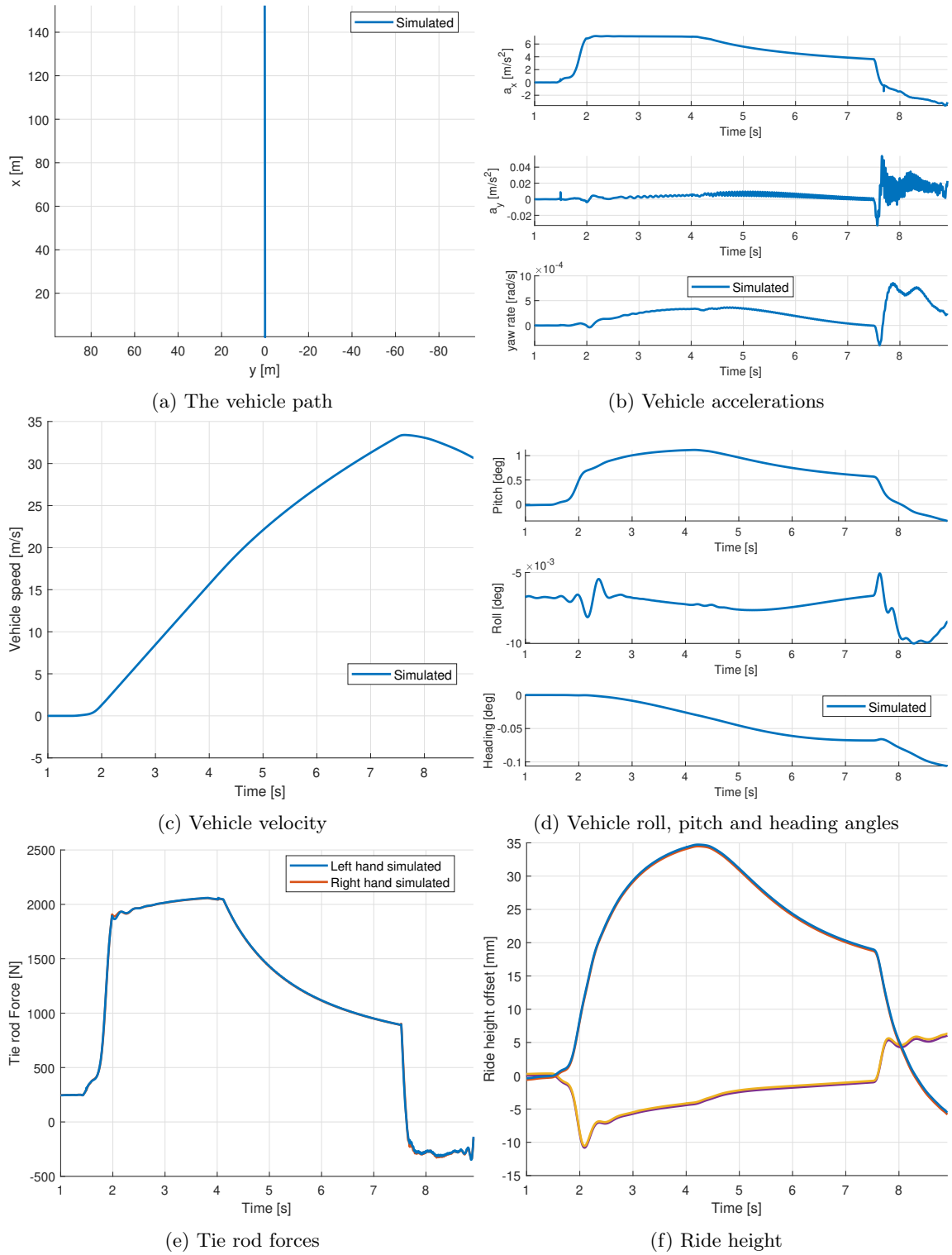

(a) The vehicle path

(b) Vehicle accelerations

(c) Vehicle velocity

(d) Vehicle roll, pitch and heading angles

(e) Tie rod forces

(f) Ride height

Figure A.4: The vehicle simulation results

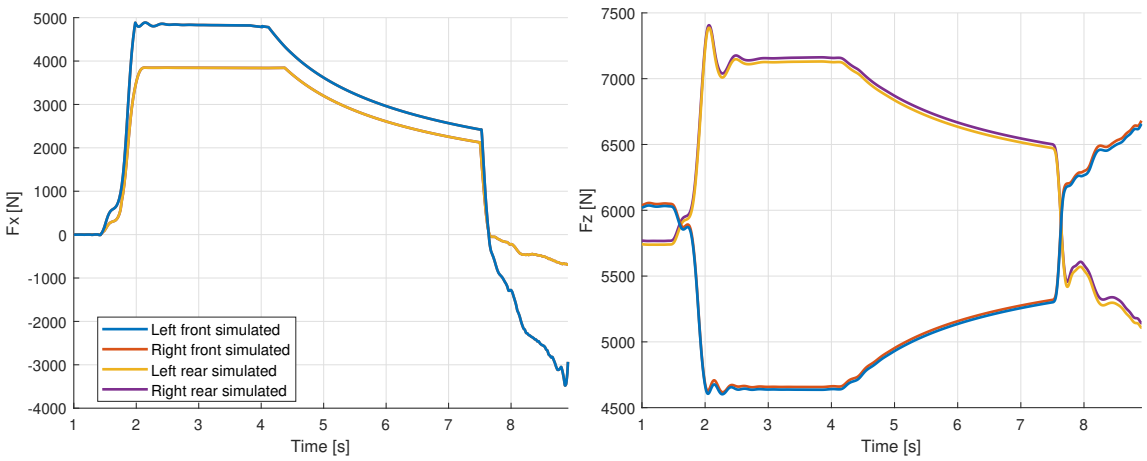

(a) Tractive force (F_x)

(b) Vertical force (F_z)

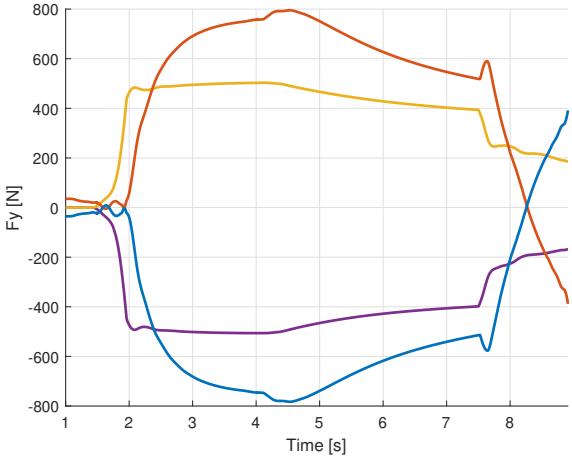

(c) Lateral force (F_y)

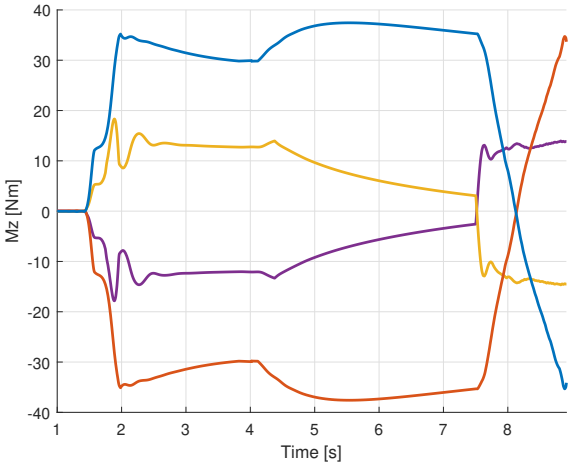

(d) Self aligning moment (M_z)

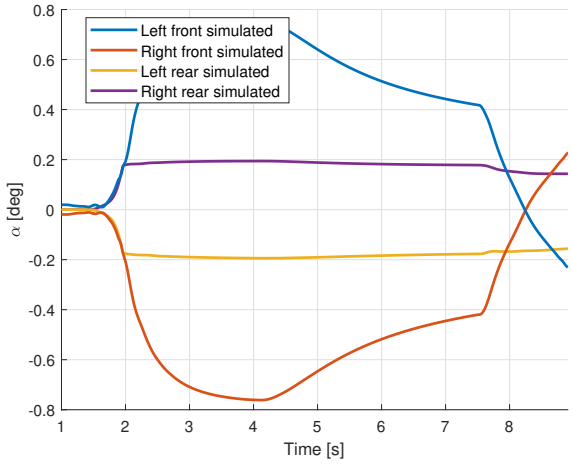

(e) Slip angle (α)

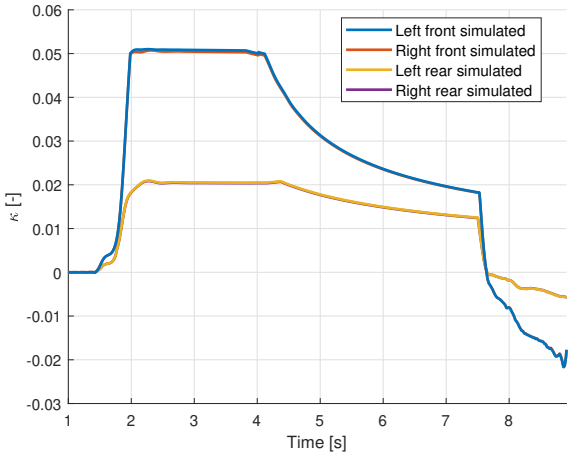

(f) Longitudinal slip (κ)

Figure A.5: The Tire simulation results

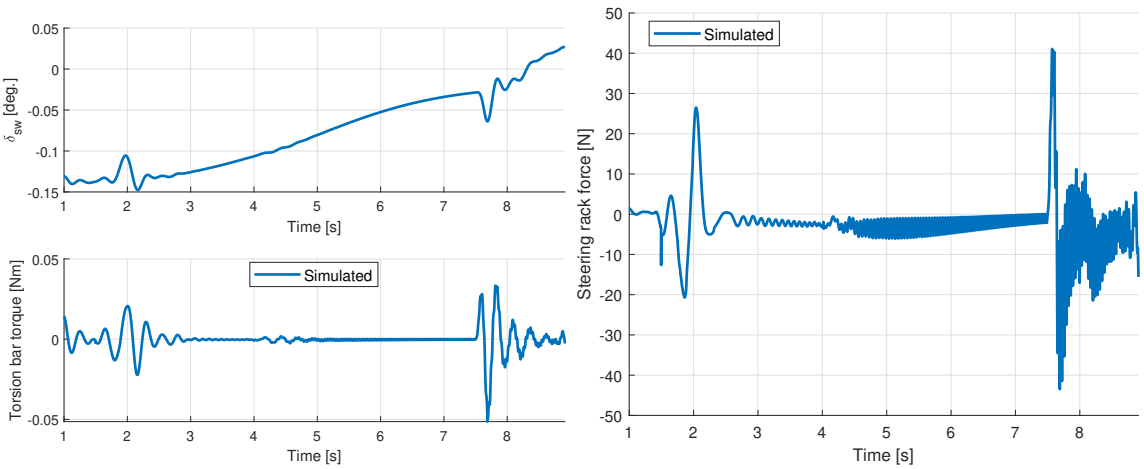

(a) Steering wheel position and torque

(b) Steering rack force

Figure A.6: The steering system simulation results

A.4 Adjusted air suspension hands off wide open throttle simulation results

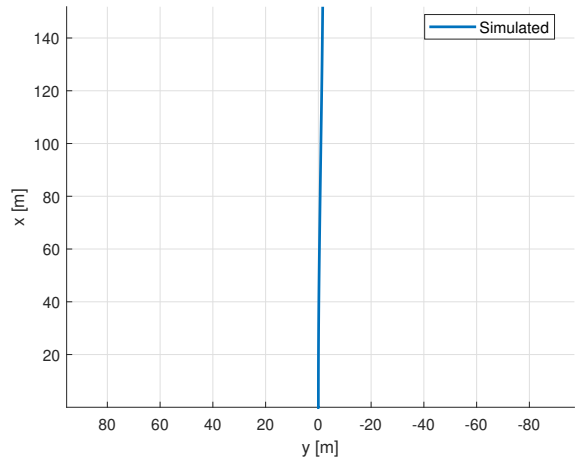

(a) The vehicle path

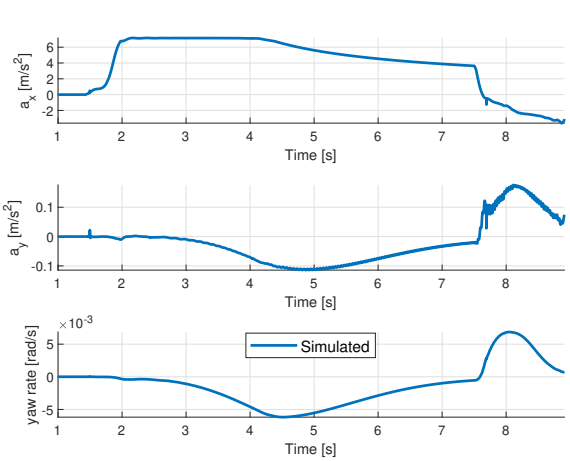

(b) Vehicle accelerations

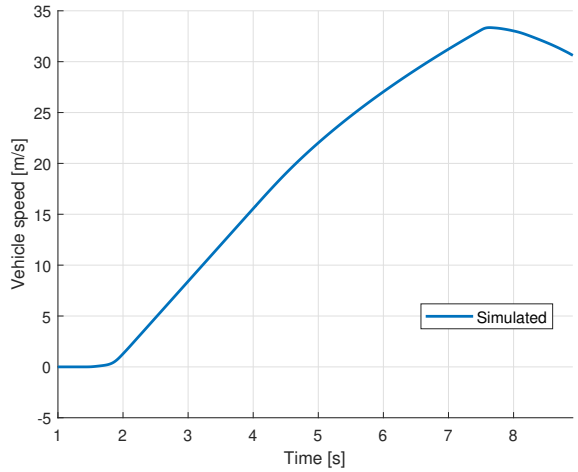

(c) Vehicle velocity

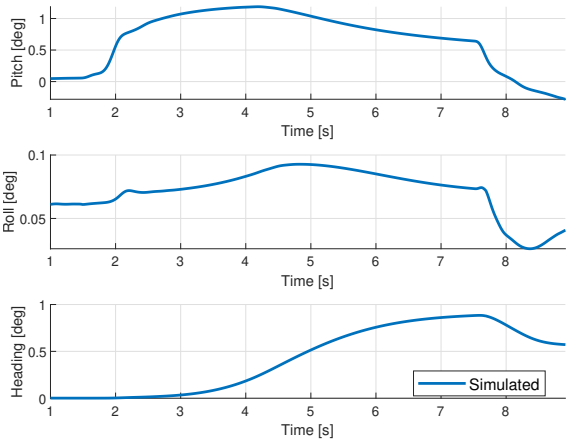

(d) Vehicle roll, pitch and heading angles

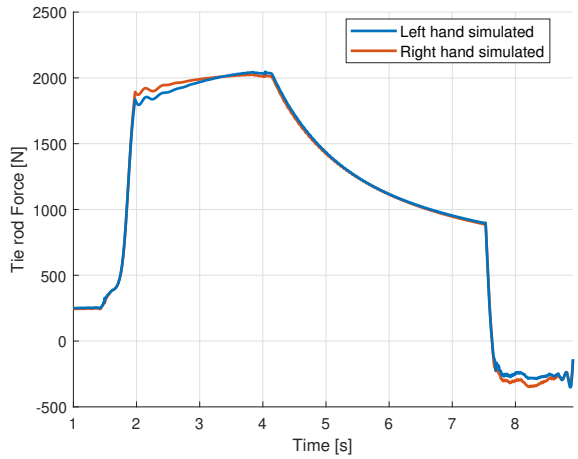

(e) Tie rod forces

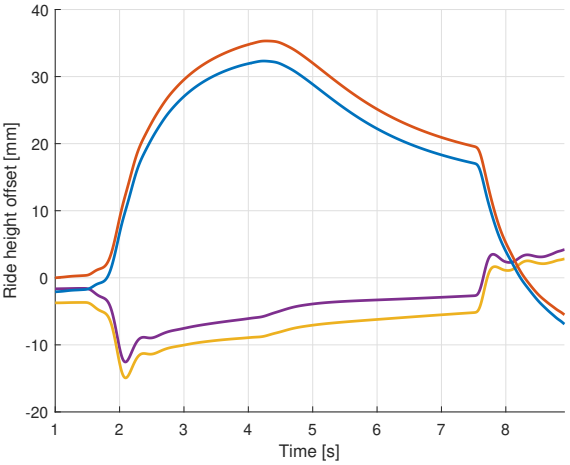

(f) Ride height

Figure A.7: The vehicle simulation results

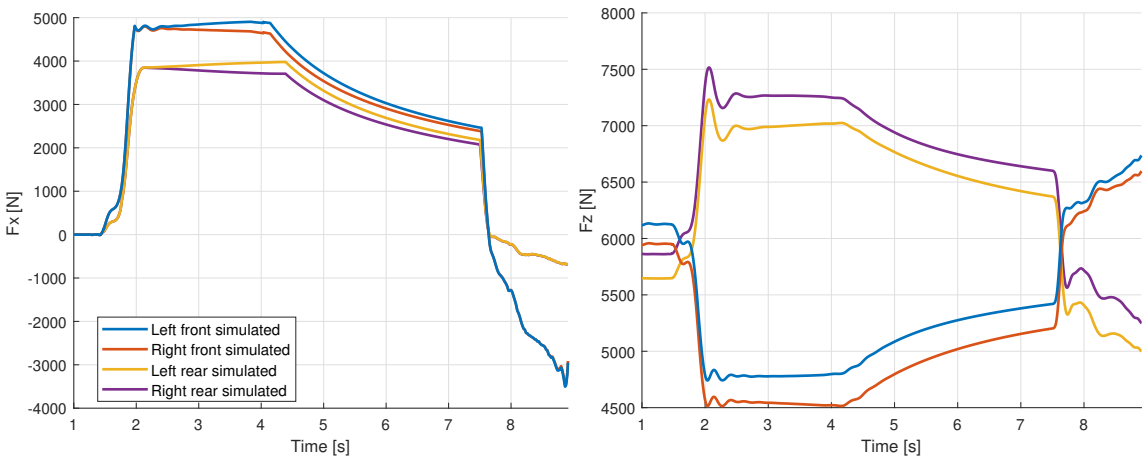

(a) Tractive force (F_x)

(b) Vertical force (F_z)

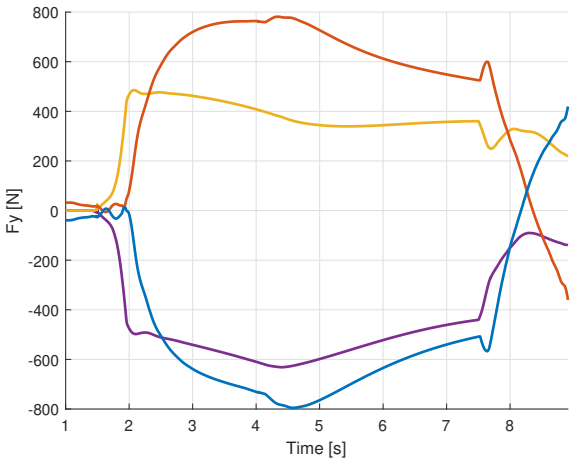

(c) Lateral force (F_y)

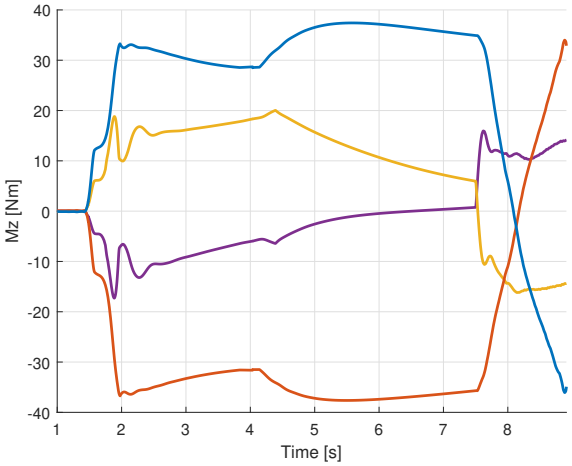

(d) Self aligning moment (M_z)

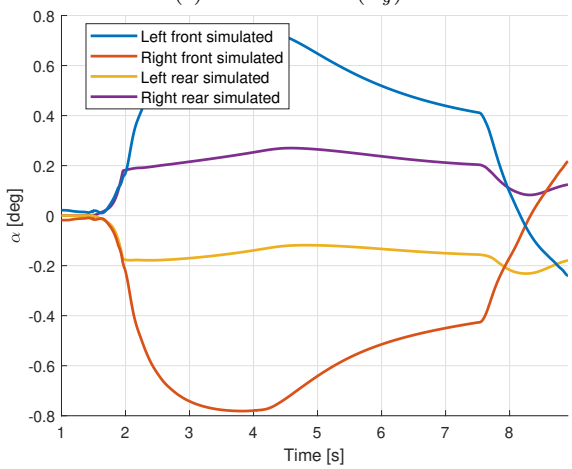

(e) Slip angle (α)

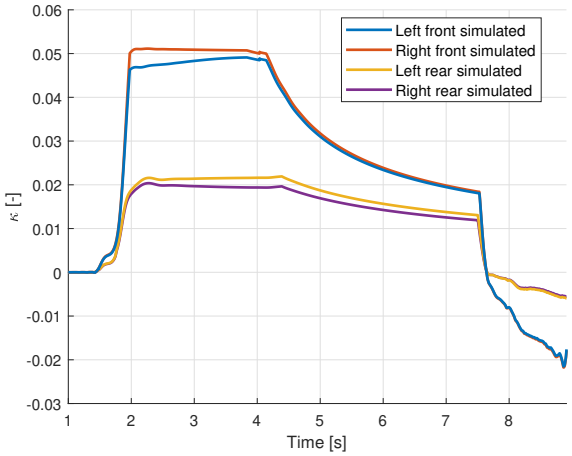

(f) Longitudinal slip (κ)

Figure A.8: The Tire simulation results

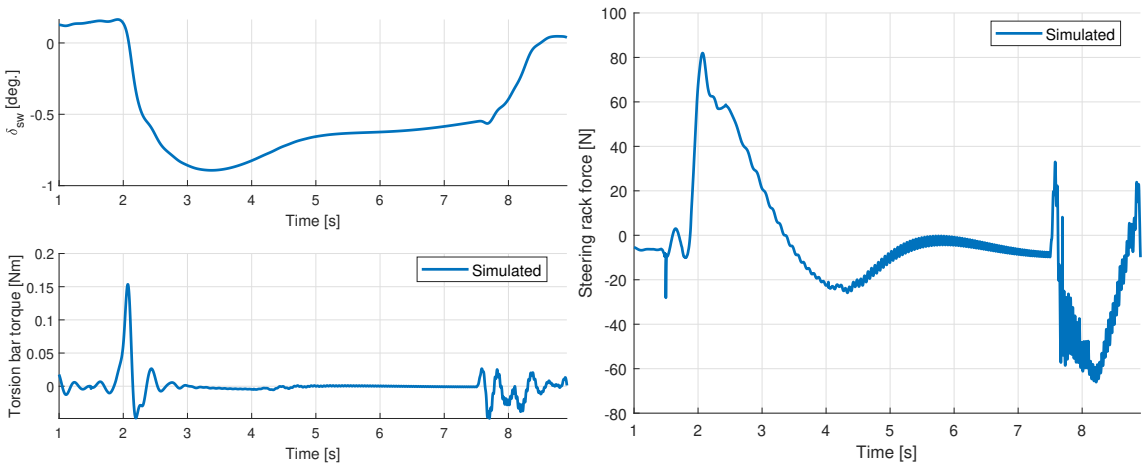

(a) Steering wheel position and torque

(b) Steering rack force

Figure A.9: The steering system simulation results